Water balance of the Aswan High Dam Reservoir

This thesis is submitted to

The Faculty of Mathematics and Natural Sciences

Kiel University

to earn the academic degree of

Doctor of Natural Science

(Dr. rer. nat.)

Dissertation submitted

by

Ahmed El.Shazli Ahmed Hussein

Born on 25.05.1977 in Aswan, Egypt

Doctor advisor and reviewer: Prof. Dr. Nicola Fohrer

Second reviewer: Prof. Dr. Hans-Rudolf Bork

Kiel University, Institute for Natural Resource Conservation

Faculty of Mathematics and Natural Sciences

Olshausenstraße 75

24118, Kiel, Deutschland.

The disputation was held on the 15th of June 2018

Acknowledgement

After praising and thanking Allah, Glorified and Exalted is He, I would like to use this little space to express my gratitude to the people without their support, this work would not have been realized.

First, I would like to thank **Prof. Dr. Nicola Fohrer**, for her support, encouragement, and advice throughout my research work.

My sincere gratitude is also extended to **Dr. Georg Hörmann,** my research supervisor, for his continuous technical support throughout my Ph.D. study. I appreciate the time and effort that he has devoted to me. His sincere help and insightful assistance and guidance have been extremely helpful to me.

A special thank goes to **Dr. Paul D. Wagner** for his kind cooperation and advice throughout my research work.

To all my colleagues at Institute for Natural Resource Conservation, Department of Hydrology and Water Resources Management, I acknowledge your support and kind companionship.

This research work could not be performed without extensive field data collection in Nile Basin. Hence, I would like to thank all those who have participated one way or another to make the data collection campaign a success. Most of all, I would like to extend my gratitude to all my colleagues in Aswan and High Dam Authority, Ministry of Water Resources and Irrigation for their continuous involvement.

Last but not the least, I am extremely grateful to my parents, brothers, and sister for their support and prayers for me.

M.Sc. Eng. / Ahmed El.Shazli Ahmed Hussein

Abstract

Egypt is an arid country with hardly any rainfall and poor underground aquifers, and it is the most downstream country traversed by the Nile River. Therefore, the River Nile is the main source for Egypt's water. In the twentieth century, the Old Aswan Dam, a reservoir with small annual storage-capacity, and many barrages were constructed across the River Nile for irrigation purposes. However, these works did not satisfy the country's needs and the desire for control of the river flow to protect Egypt from high floods and drought and to meet the annual downstream requirements of water for sustainable irrigated agriculture. So, it was decided to build the Aswan High Dam as a long-term storage reservoir and as a part of a multipurpose project.

Now, Aswan High Dam Reservoir is of fundamental strategic importance for sustaining water demand in Egypt because it secures the annual agreed quota from the Nile River which is 55.5 km^3. Optimum management of the Aswan High Dam Reservoir (AHDR) requires a better understanding of the hydrological aspects of the reservoir area, and an accurate estimating of the different terms of the hydrological budget.

This study aims to discuss the hydrological dimensions of the Aswan High Dam Reservoir. It examines the sedimentation in the reservoir and detects the changes in the storage capacity and the morphology of the AHDR because of sediment deposits. Also, a digital elevation model for the reservoir is generated and a new elevation–area–capacity curve is obtained. Water loss by evaporation is one focus of this research. The evaporation rate is estimated by water balance method and sixteen alternative evaporation methods. Furthermore, the study discusses the interaction between groundwater and surface water in the reservoir area using cross-correlation analysis, and the water loss from the reservoir by seepage and absorption.

Zusammenfassung

Ägypten ist ein Land mit aridem Klima und geringen Grundwasservorräten, dessen Wasserressourcen vor allem vom Nil bestimmt werden.

Im frühen zwanzigsten Jahrhundert wurden zuerst der alte Assuan-Damm und viele kleine Staudämme gebaut mit einer relativ kleinen Speicherkapazität, die hauptsächlich zur Bewässerung genutzt wurde. Diese Bauwerke reichten jedoch weder aus, um die Wasserversorgung noch den Hochwasserschutz sicher zu stellen. Zur Lösung dieser Probleme wurde deshalb der Assuan-Staudamm gebaut, der jährlich 55.5 km^3 Wasser zur Verfügung stellt.

Das optimale Management des Assuan-Stausees erfordert ein besseres Verständnis der Hydrologie des Stauseebereiches und eine genaue Erfassung der verschiedenen Komponenten der Wasserbilanz.

Ziel dieser Arbeit war es deshalb, die Hydrologie des Assuan-Stausees genauer zu erfassen. Dazu gehört der Sedimenttransport im Assuan-Stausee, die Änderungen der Lagerungskapazität und die durch Sedimentablagerungen veränderte Morphologie des Stausees. Außerdem wurde ein neues, digitales Höhenmodell für den Stausee erzeugt und eine neue Höhenbereichs-Höhenkapazitätskurve erstellt.

Ebenfalls berechnet wurde der Wasserverlust durch die Verdunstung mit Hilfe der Wasserhaushaltsmethode und von sechzehn weiteren Verdunstungsformeln.

Schließlich werden Ansätze zur Berechnung der Wechselwirkung zwischen Grundwasser und Oberflächenwasser mit Hilfe der Kreuzkorrelationsanalyse vorgestellt.

Table of Contents

List of Figures

List of Tables

1 Introduction

1.1 Background

The Nile River supplies more than 95% of Egypts water demand. Thus it serves as a lifeline to almost the whole of Egypt. Long-term storage was recommended to control the flow of the river, supply water for irrigation throughout the year, and to double the agricultural yield. In 1952 the Egyptian government decided to construct a dam to regulate the flow of the river. The construction of the Aswan High Dam (AHD) began in 1960 and was completed in 1968. The construction of the AHD entailed the development of the Aswan High Dam Reservoir (AHDR), which is considered one of the largest man-made reservoir in the world based on the water storage capacity.

The maximum capacity of the AHDR was estimated before 1964 by the Ministry of Water Resources and Irrigation (MWRI) of Egypt as 162 km^3 at the maximum water level of 182 m a.s.l. (Abu Zeid and El-Shibini 1997). The reservoir has an area of 6540 km^2 (Elsawwaf et al. 2010), a length of 500 km, of which 350 km lie in Egypt and 150 km in Sudan (Omar and El-Bakry 1981), and an average width of 12 km.

The average annual flow of the Nile River at Aswan for the period 1870–1957 was about 84 km^3. 70% of the mean annual flow comes from the Ethiopian Highlands through the Blue Nile and Atbara Rivers and 30% from the White Nile River (Mobasher 2010). About 90% of the Nile River water during the flood period (August–November) comes from the Blue Nile and Atbara Rivers, while following this period most of the water comes from the White Nile River and its tributaries in the riparian countries as shown in Fig 1-1 (Mobasher 2010).

The AHDR is located in the hyper-arid zone in southern Egypt and northern Sudan. The reservoir extends between latitudes 21˚02 to 23˚58' N and longitudes 30˚37' to 32˚55' E (Elba *et al.* 2014). AHDR, in general, is surrounded by rocky terrain and peneplains of Nubian sandstone. To the west lies the great Sahara Desert and to the east is the Eastern Desert extending to the Red Sea (Raheja 1973). The slope of the reservoir shoreline is steeper on the rocky or stony, mountainous, eastern shore than on the flatter, wider, sandy, western one (El Shahat 2000). Precipitation is extremely scarce in the AHDR area. The mean wind speed over the year is in the range of 15 to 19 km h^{-1}, and its direction is NW-NE (Elshemy 2010).

From a hydrogeological point of view, the Nubian sandstone formation is the main aquifer in the study area. The river cuts into the sandstone strata. Therefore the water level of the lake and the groundwater table are related.

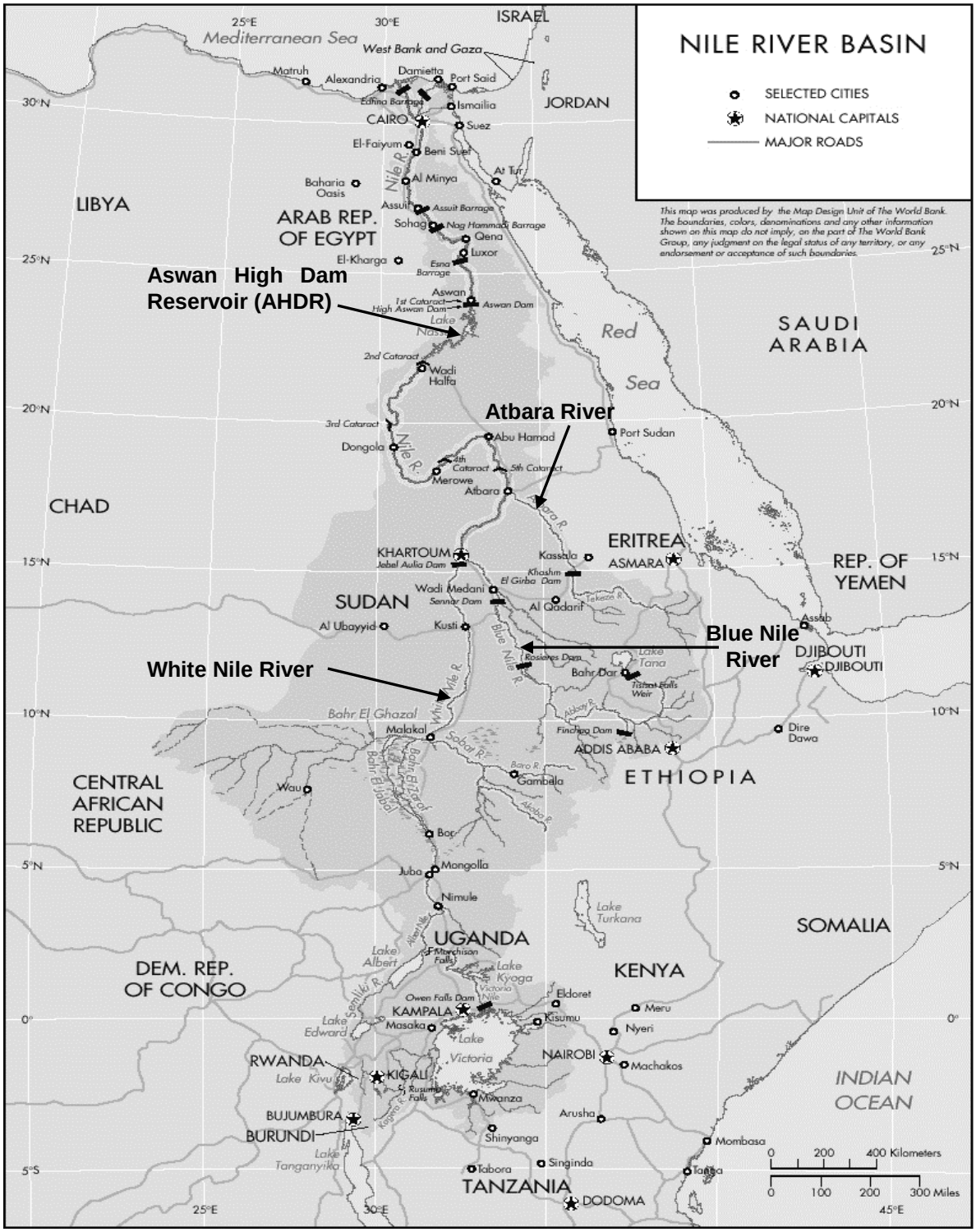

Figure 1-1 Location map of the Nile River and the AHDR (http://siteresources.worldbank.org)

Sediment transport, evaporation losses and the interaction between the groundwater and surface water in the reservoir region will be studied to determine the influence of these three processes on the hydrological budget of the reservoir.

Sedimentation is the greatest cause of loss of storage capacity in reservoirs. The annual sediment load deposited by the Nile River into the AHDR ranges from 50 to 228 × 10^6 tons (Abul-Atta, 1978).

Evaporation loss decreases the water budget of the AHDR. Preliminary studies for the reservoir design stated that the annual evaporation was measured using half of Piche evaporimeter as 2.75 m yr^{-1} (WRRI, 2007). Groundwater inflow and leakage are important components of the hydrologic budget. Preliminary studies for the reservoir design declared that the seepage from the reservoir was estimated at 0.5 × 10^9 to 1.0 × 10^9 m^3 yr^{-1}.

1.2 Motivation

Water is a crucial element for human beings and natural systems. In addition to rapid population growth, Egypt now faces enormous challenges due to its limited water resources represented mainly by its fixed share of the Nile water. So that, the AHDR represents the main source of fresh water in Egypt.

Optimum management of the AHDR requires a better understanding of the hydrological aspects of the reservoir area, and an accurate estimation of the different terms of the hydrological budget. Furthermore, it is of utmost importance to properly understand the changes that take place in the reservoir.

1.3 Objectives of the study

Water balance procedures, one of the main issues in hydrology, are a means of solution of important theoretical and practical hydrological problems (Sokolov and Chapman, 1974). This study focuses on the water budget of the AHDR. Studying the water balance of the AHDR requires examining three main points. These points are :

1- the change in the storage capacity of the AHDR because of sediment entry,

2- the evaporation rate from the reservoir,

3- and the exchanged water volume between groundwater and surface water in the reservoir area.

1.4 Content and structure of the thesis

This thesis consists of three chapters. The first chapter is about the development of the storage capacity and the morphology of the AHDR. The objectives of this chapter are: (1) to establish a DEM for the present situation of the AHDR; (2) to obtain a new elevation–area–capacity curve for the AHDR based on the DEM; and (3) to detect the changes in storage capacity and morphology of the reservoir caused by sedimentation.

The second chapter deals with the water losses from the reservoir by evaporation. This chapter discusses three items. These items are: (1) determine the water losses from the AHDR using the water balance method; (2) determine the evaporation rate from the AHDR using 16 alternative evaporation/evapotranspiration methods; and (3) quantify the relation between evaporation rates determined by the evaporation/evapotranspiration methods and the evaporation rate estimated by the water balance method.

The third chapter discusses the water losses by infiltration from the reservoir and the interaction between groundwater and surface water in the reservoir region. The elements of this chapter are: (1) using cross-correlation between the groundwater tables in the boreholes and the water levels in the Nasser Lake (NL) to find the boreholes with a connection to the water level; (2) using the boreholes to estimate the seepage volume from the NL to the groundwater; (3) estimate the volume of water, which is needed to saturate the dry rock.

2- Development of storage capacity and morphology of the Aswan High Dam Reservoir

Journal article (published)
Authors: El-Shazli, A., & Hoermann, G.
Journal: Hydrological Sciences Journal.
Volume: 61, 2016 - Issue 14
Date of publication: 25 Jul 2016
Reprinted with permission from Taylor & Francis from:
El-Shazli, A., & Hoermann, G. (2016). Development of storage capacity and morphology of the Aswan High Dam Reservoir. Hydrological Sciences Journal, 61(14), 2639-2648.

2 Development of storage capacity and morphology of the Aswan High Dam Reservoir

Abstract:

A digital elevation model (DEM), as well as satellite images, was used to detect the changes in the morphology and storage capacity of the Aswan High Dam Reservoir (AHDR) over the past five decades. Study findings indicate that the total storage capacity of the AHDR estimated by the DEM decreased by 12%. This decrease is mainly in the live and the dead storage capacities. The morphology of the reservoir changed in the southern part and at the entrance of the lacustrine part. A gradual conversion of the entrance to the riverine part was observed. The surface area of the AHDR decreased at low water levels because of sedimentation. The average reduction of the surface area between water levels of 140 and 168 m a.s.l. is about 15%, which is equivalent to almost 10 km^3.

Keywords: Aswan High Dam Reservoir (AHDR), Landsat, Sediment, Digital Elevation Model (DEM), Morphology

2.1 Introduction

Manmade reservoirs are basins filled with water continually in use by humans (Jorgensen et al. 2005). Large reservoirs are utilized to develop and manage natural resources to sustain economic growth (Takeuchi 1998). Reservoir projects are constructed for many purposes such as municipal and industrial water supply, irrigation, hydropower, flood control and recreation. At the end of the twentieth century, there were about 45 000 large dams in more than 140 countries (World Commission on Dams 2000). Worldwide, about 70% of riversare obstructed by large reservoirs (Nilsson et al. 2005).

Reservoir sedimentation is normally considered an undesirable but inevitable consequence of water storage (Palmieri et al. 2001). Sedimentation is the greatest cause of loss of storage capacity in reservoirs (Schleiss et al. 2014). Continuous sediment deposition increases bed elevation and forms a new delta that can hinder navigation (El-Manadely et al. 2002).

Monitoring the changes that take place in large reservoirs because of sedimentation using only traditional methods is difficult and impractical. Fortunately, remote sensing resources that are currently available free of charge represent a great opportunity to support monitoring and study of hydrological and hydraulic processes (Abileah et al. 2011). Compared with the traditional method (land and hydrographic survey), remote sensing can be affordable, easy to use and requires less time to analyse the data, (Peng *et al.* 2006). Over the last twenty years, remote sensing has been used to estimate the water storage in the large reservoirs and lakes (Gao *et al.* 2012). Remote sensing data is two-dimensional in nature. Therefore, some effort is required to design or modify hydrological models that will accept this two-dimensional input (Rango 1994). Compared with the traditional method (land and hydrographic survey), remote sensing can be affordable, is easy to use and requires less time to analyse the data, (Peng et al. 2006). Over the last 20 years, remote sensing has been used to estimate water storage in large reservoirs and lakes (Gao et al. 2012). Remote sensing data are two-dimensional in nature. Therefore, some effort is required to design or modify hydrological models that will accept this two-dimensional input (Rango 1994).

Smith et al. (1983) employed Landsat imagery for the period 1972–1980 for instantaneous monitoring of surface turbidity of the southern portion of the Aswan High Dam Reservoir (AHDR) during the flood period. They found that the accumulation of sediment deposits throughout the flood period was correlated intimately with surface turbidity. Also, regions with high surface turbidity showed deeper sediment deposits, as compared to regions with low surface turbidity. They prepared three-dimensional plots of the southern portion of the reservoir where the sedimentation arises. Elba et al. (2014) used 20 imagery sets for the years 1984–1999, old topographic maps of the AHDR area and bathymetric survey data of the year 2007 to generate a DEM. Elba et al. (2014) estimated the deposited sediment volume as 7 km^3, but they did not show any illustrations of sediment distribution in the reservoir. Jain et al. (2002) used the remote sensing approach for the years 1996–1997 to estimate the sediment in the Bhakra Reservoir located on the Satluj River in the foothills of the Himalayas. This study showed that the average sedimentation rate for 32 years (1965–1997) was 25.23 $hm^3\ year^{-1}$. Peng et al. (2006) chose the Fengman Reservoir in China as a case study to estimate a new storage curve based on Landsat data for the period 1973– 2000. The results

showed that the new estimated curve is in close agreement with the 1956 design curve. Goel et al. (2002) used nine satellite scenes for 1996/1997 to estimate the actual annual storage loss in the Bargi Reservoir because of sedimentation. The results indicated that the loss rate in the area under study was 229.03 m^3 km^{-2} $year^{-1}$.

The AHDR represents the main source of Egypt's freshwater. Therefore, knowledge of the characteristics of the AHDR is essential to apply appropriate management approaches. Furthermore, it is of the utmost importance to understand properly the changes that take place in the reservoir. The objectives of this study are: (1) to establish a DEM for the present situation of the AHDR; (2) to obtain a new elevation–area–capacity curve for the AHDR based on the DEM; and (3) to detect the changes in storage capacity and morphology of the reservoir caused by sedimentation.

2.2 Research Site

The AHDR is the third largest manmade reservoir in the world. It was formed as a result of the construction of the Aswan High Dam (AHD) across the Nile River. It is located in the hyper-arid zone in southern Egypt and northern Sudan. The reservoir extends between latitudes 21°02′–23° 58′N and longitudes 30°37′–32°55′E (Elba et al. 2014).

The slope of the reservoir shoreline is steeper on the rocky or stony, mountainous, eastern shore than on the flatter, wider, sandy, western one (El Shahat 2000). The reservoir is subdivided into two parts; a riverine part and a lacustrine part, as shown in Fig. 2-1.

The maximum capacity of the AHDR was estimated before 1964 by the Ministry of Water Resources and Irrigation (MWRI) of Egypt as 162 km3 at the maximum water level of 182 m a.s.l. (Abu Zeid and El- Shibini 1997).

The reservoir has an area of 6540 km2 (Elsawwaf et al. 2010), a length of 500 km (350 km of which lie in Egypt and 150 km in Sudan) (Omar and El- Bakry 1981) and an average width of 12 km. The total capacity of the lake comprises: (a) dead storage capacity of 31.6 km3 up to 147 m a.s.l. designed for the sediment deposits; (b) live storage capacity amounting to 90.4 km3 between 147 and 175 m a.s.l. to guarantee the annual water requirements, and (c) flood control capacity of 40 km3 between 175 and 182 m a.s.l. (Ibrahim et al. 2011).

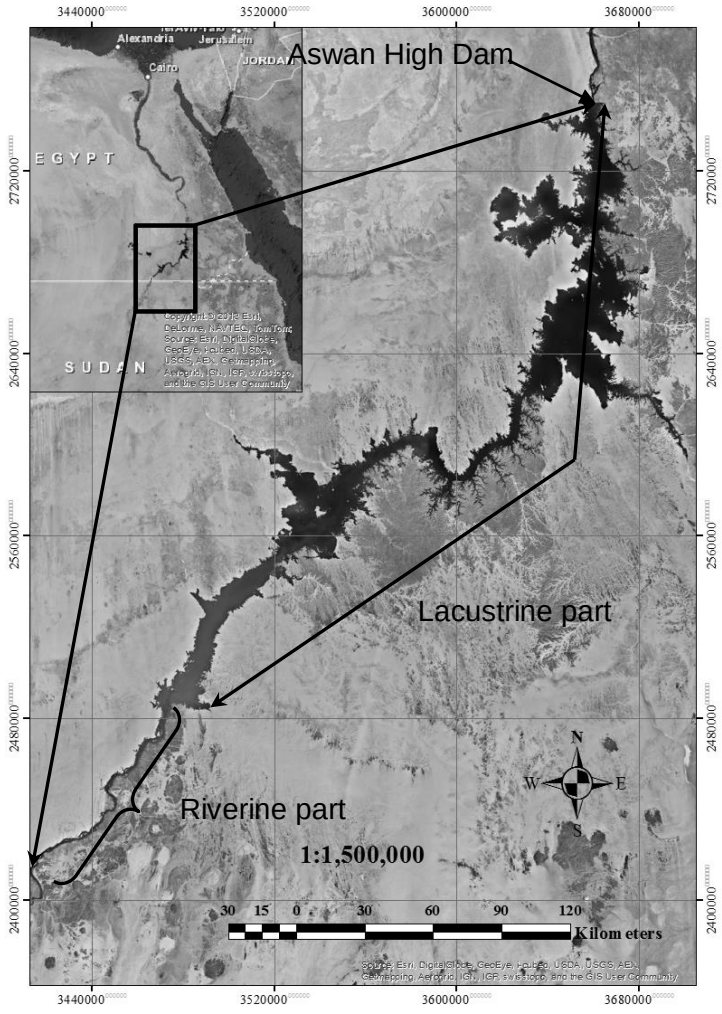

Figure 2-1 Location map of the AHDR (ESRI, 2014)

The average annual flow of the Nile River into the AHDR for the period 1965–2010 was about 73 km^3 (based on data from MWRI). The flow is measured at Dongola station, 780 km upstream of the AHD. 70% of the mean annual flow comes from the Ethiopian Highlands through the Blue Nile and Atbara Rivers and 30% from the White Nile River. About 90% of the Nile River water during the flood period (August–November) comes from the Blue Nile and Atbara Rivers, while following this period most of the water comes from the White Nile River and its tributaries in the riparian countries (Mobasher 2010).

The annual sediment load deposited by the Nile River into the AHDR ranges from 50 to 228 million tons (Abul-Atta, 1978). As a result of the erodible upland terrains, high sediment supply and high runoff, approximately 97% of the annual suspended-sediment

load originates from the Ethiopian Highlands during the flood period through the Blue Nile and Atbara Rivers (Woodward 2008), as depicted in Fig. 2-2.

The water level of the reservoir started to increase on construction of the AHD in 1964. In 1975, the reservoir level reached the full storage level (175 m a.s.l.) and remained almost stable up to 1982. From 1983 to 1989 the storage level decreased, to 150.62 m a.s.l. in 1988, because of drought seasons. From 1998 to 2001 the reservoir was exposed to successive high floods and the water level approached the maximum storage level in November 1999 (181.60 m a.s.l.). From 2002 up to 2012, the level fluctuated between 168 and 178 m a.s.l., as shown in Fig. 2-3.

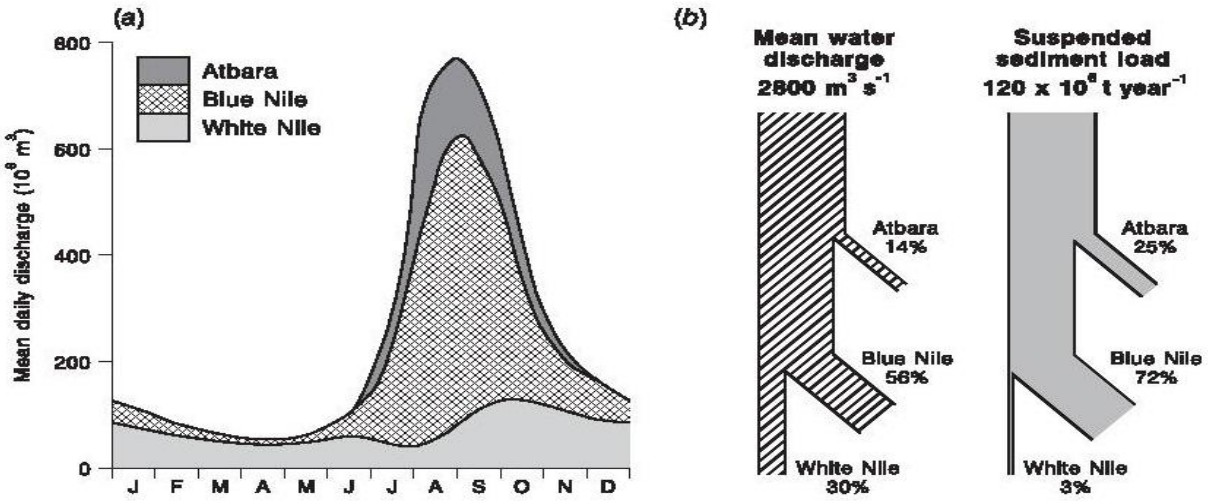

Figure 2-2 (a) Typical annual flow regime of the Nile River at Aswan and the contributions from the three major tributary basins. (b) The discharge and suspended sediment budget of the Nile (after Woodward, 2008, with permission from Wiley)

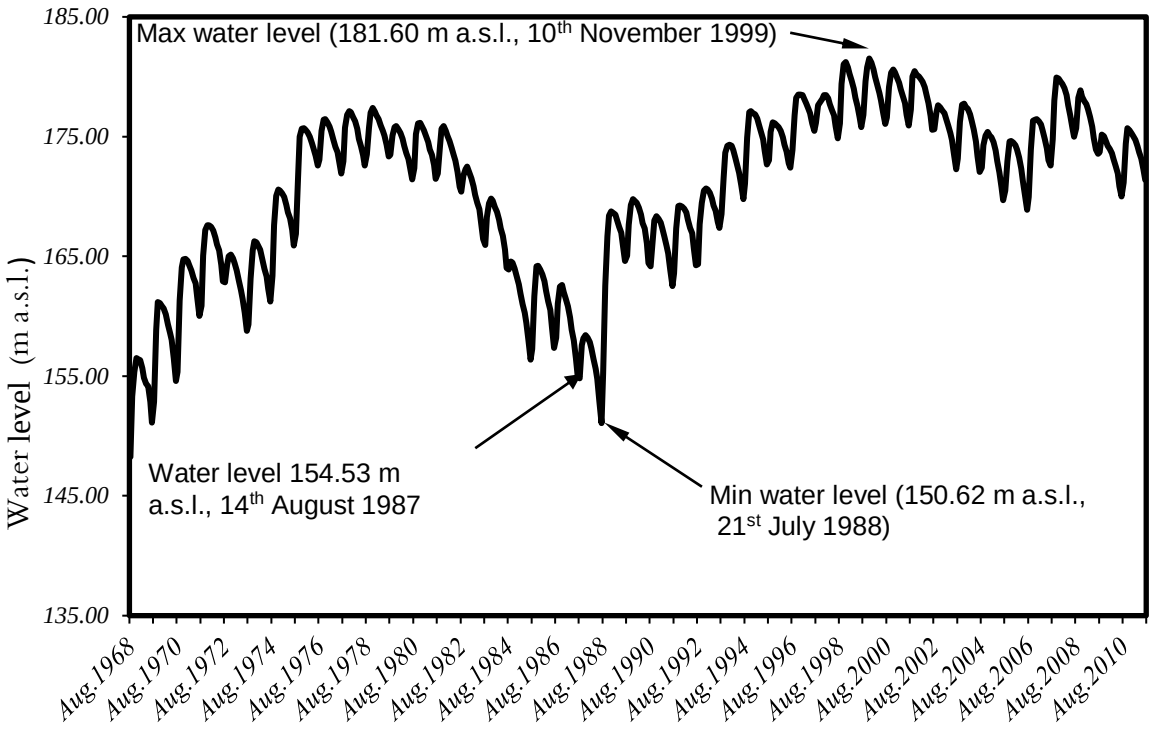

Figure 2-3 Water level upstream AHD from 1968 till 2010 based on data from the MWRI.

2.3 Material and Techniques

Landsat imagery with a spatial resolution of 30 m, the digital contour map of the AHDR area before the dam construction and bathymetric data were employed to generate the DEM, as depicted in Fig. 2-4.

2.3.1 Satellite Images

The main reason for using Landsat imagery in this study is its ability to yield instantaneous images of the shorelines of the AHDR as the water levels vary over time, and this is considerably difficult to achieve by ground survey.

The reservoir is covered by the US satellites Landsat 4, 5, 7 and 8 through three sets of images identified by path/row numbers 174/44, 175/44 and 175/45. The minimum and maximum water levels represented on satellite images for the period 1984–2013 were 154.53 and 181.60 m a.s.l. On May 2003, Landsat 7 suffered a failure leading to loss of 22% of any given scene (http://land sat.usgs.gov/productsslcoffbackground.php).

Also, the reservoir is not covered by satellite images for the period 1992– 1997. The Landsat data are listed by date in ascending order in Table 1. Band 4 of Landsat 4, 5 and 7, as well as band 5 of Landsat 8, were analysed to delineate the boundaries of the AHDR. Bands 4 and 5 (the near infrared bands with wavelengths of 0.77–0.90 μm and 0.85–0.88 μm, respectively) emphasize biomass content and shorelines as reported on the Landsat website (http://landsat.usgs.gov/ best_spectral_bands_to_use.php.).

ENVI 4.7 was used to mosaic (overlay) the satellite scenes that have overlapping areas to create one scene covering the whole reservoir area at an individual water level. Then the reservoir area was delineated by ISODATA unsupervised classification. The output of the reservoir delineation in ENVI 4.7 software was imported into ArcGIS and transformed to a shapefile. This shapefile was used to create the main polyline representing the shoreline of the reservoir at a particular water level. This process was conducted for the imagery sets representing the reservoir at different water levels as shown in Fig. 2-5(b). Every polyline was utilized as a contour line in the interpolation process to create the DEM.

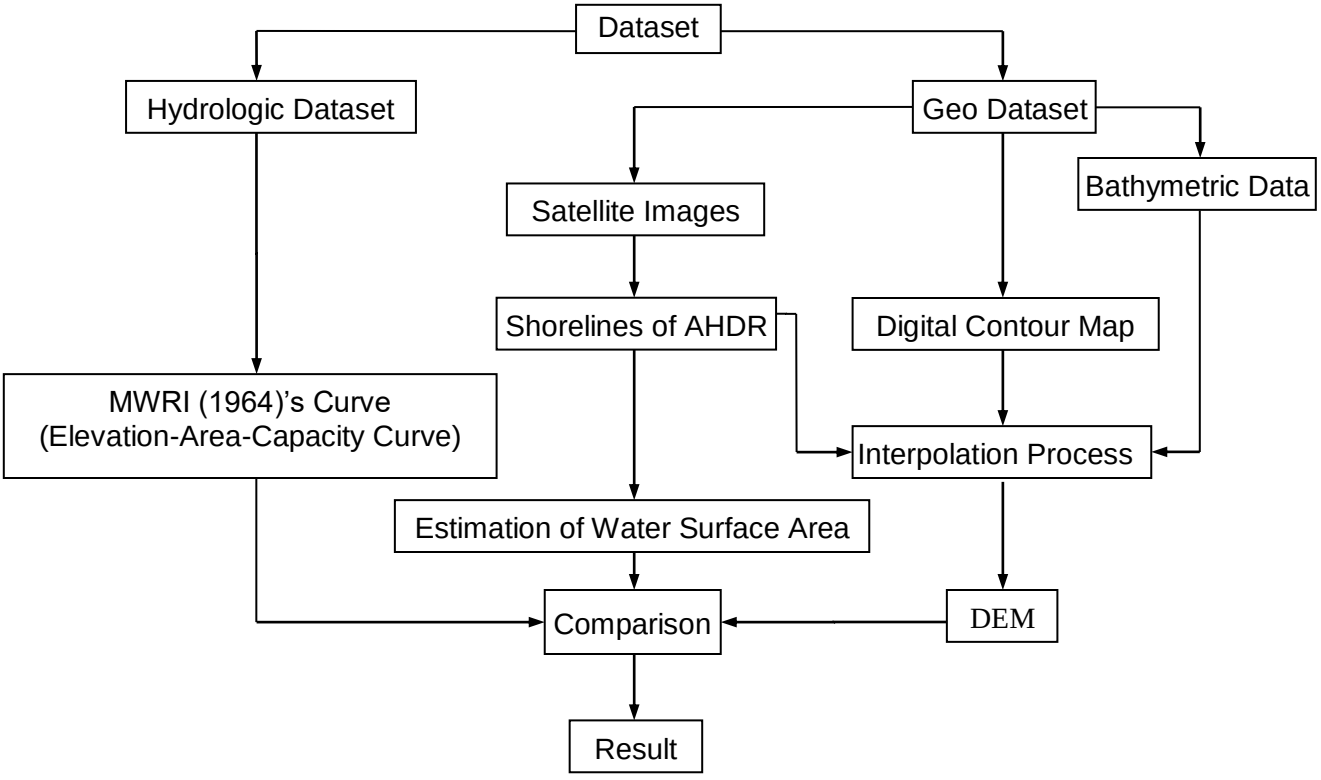

Figure 2-4 Flowchart of the methodology

Table 2-1 List of utilized imagery with acquisition dates and the corresponding water levels at AHDR

No.	Acquisition Dates	Reservoir Elevation (m.a.s.l)	Path/Row
1	02.06.1984	166.24	174/44
2	31.10.1984	164.34	175/44 and 175/45
3	28.01.1985	162.44	174/44
4	23.02.1986	162.87	174/44
5	03.02.1987	161.18	174/44
6	10.02.1987	160.97	175/44 and 175/45
7	14.08.1987	154.53	174/44
8	01.03.1988	156.96	174/44
9	24.03.1988	156.16	175/44 and 175/45
10	01.01.1989	168.65	174/44
11	06.01.1989	168.58	175/44 and 175/45
12	29.08.1990	165.00	175/44 and 175/45
13	30.08.1990	165.08	174/44
14	12.08.1998	175.67	174/44
15	03.11.1999	181.51	174/44
16	10.11.1999	181.60	175/44 and 175/45
17	14.01.2000	180.62	174/44
18	10.03.2000	179.44	174/44
19	14.06.2000	177.09	174/44
20	10.09.2000	178.82	174/44
21	04.11.2000	180.59	175/44 and 175/45
22	08.04.2013	173.47	174/44
23	24.05.2013	172.94	175/44 and 175/45
24	09.06.2013	172.54	175/44 and 175/45
25	18.06.2013	172.38	174/44
26	20.07.2013	171.80	174/44
27	27.07.2013	171.65	175/44 and 175/45
28	28.08.2013	174.04	175/44 and 175/45
29	13.09.2013	175.82	175/44 and 175/45

2.3.2 Digital Contour Map

The digital contour map of levels 120–150 m a.s.l. was developed from 1:100 000 topographic maps produced in 1960 (before the AHD construction) shown in Fig 2-5(a). The digital map is utilized because the reservoir below a water level of 154 m a.s.l. is not represented by the satellite images.

2.3.3 Bathymetric survey data

The reservoir is surveyed almost every year by the MWRI. The bathymetric survey process is conducted by using Differential Global Positioning System (DGPS) and a digital echo-sounder. Most parts of the reservoir were surveyed in the years 2011–2012, except for some portions in the northern part of the reservoir as shown in Fig 2-5(b).

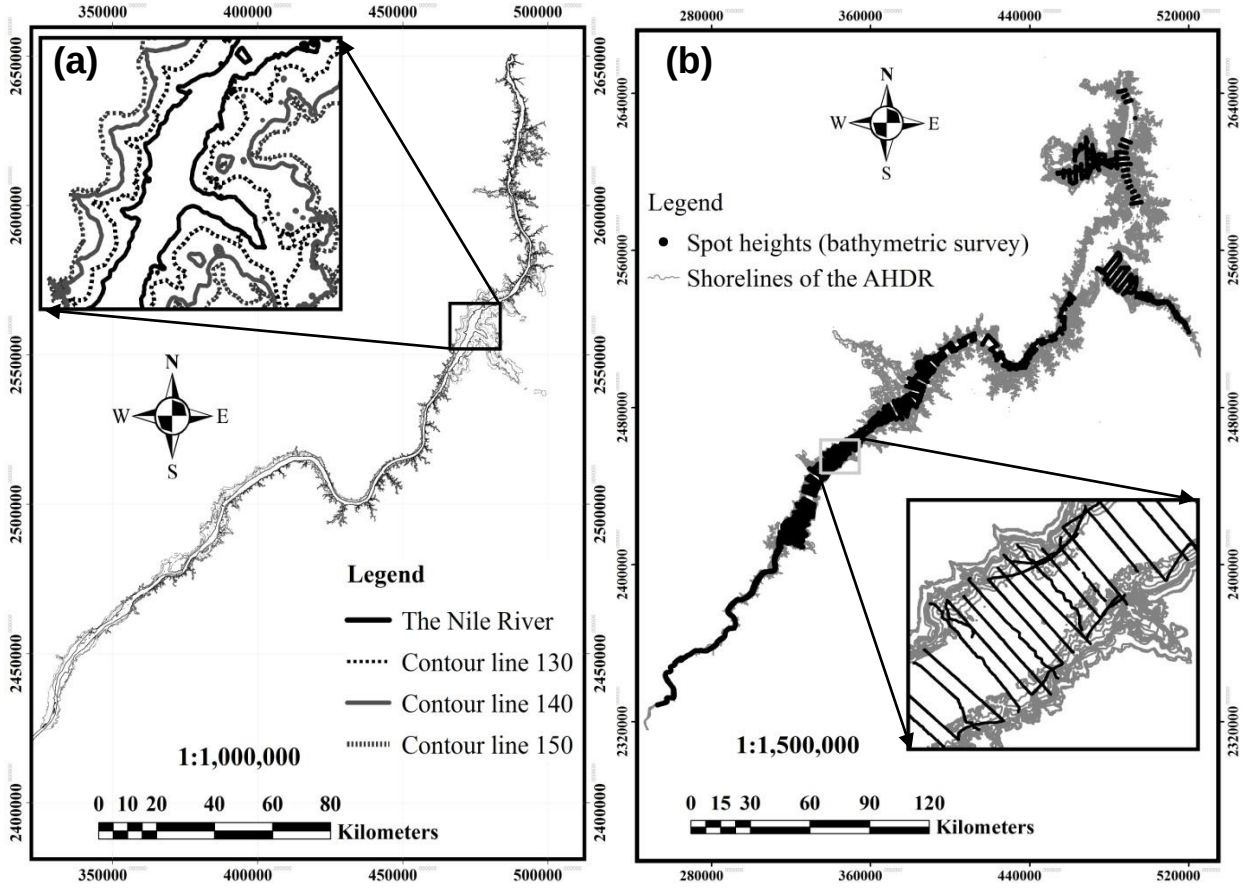

Figure 2-5 (a) Digital contour map of the AHDR area before the Aswan High Dam construction based on data from MWRI. (b) Bathymetric survey data and boundaries of the AHDR extracted from satellite images for the period 1984-2013

These parts are not exposed to sedimentation, and their morphology did not change. The bathymetric survey data were classified into categories according to the bed elevation of the reservoir to fill the gaps (non-surveyed areas) between the surveyed areas. Furthermore, because of the sedimentation in the southern part of the AHDR, the bathymetric data were used to adjust the contour lines of the digital map.

2.3.4 Interpolation Process

All contour lines and spot heights were combined to create a DEM by using the Topo to Raster interpolation method in ArcGIS software.

The Topo to Raster tool is an interpolation method particularly designed to generate hydrologically correct DEMs (ESRI 2014).

2.4 Results and Discussion

The result of the interpolation process is a DEM of the AHDR represented as a raster. The DEM covers the area of the reservoir with a 25 m × 25 m grid spatial resolution. The new elevation–area–capacity curve based on the DEM was drawn to discover the changes that occurred in the reservoir.

2.4.1 Storage Capacity

As shown in Fig 2-6, the water volume of the AHDR estimated by the DEM at an elevation of 182 m a.s.l. is about 142.0 km^3. The dead storage capacity is estimated at 25 km^3 while the live storage capacity located between the levels 147 and 175 m a.s.l. is estimated as 78.0 km^3. The flood control capacity is 39 km^3 between levels 175 and 182 m a.s.l.

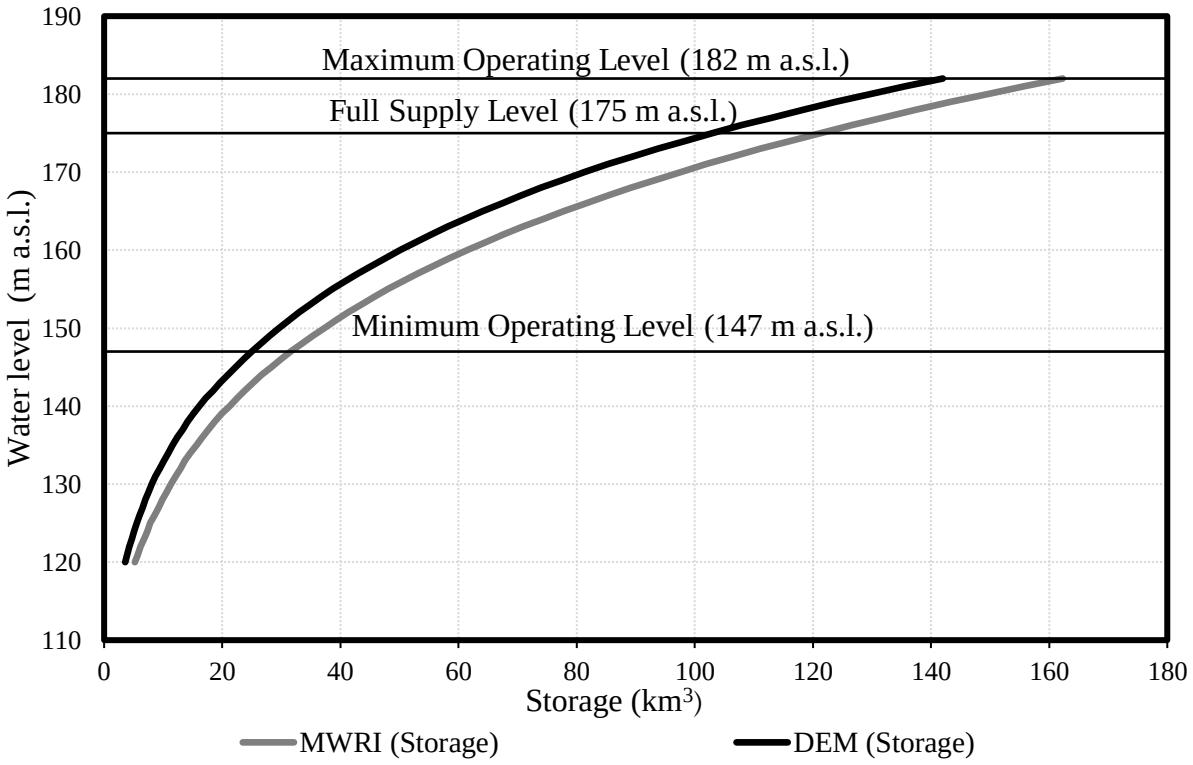

Figure 2-6 Comparison of the two storage curves MWRI (1964) and DEM

The main cause for the loss of about 12% of the storage capacity is sediment deposition. This loss of storage capacity occurred mainly in the live and the dead storage zones and slightly in the flood control zone. Widening of the reservoir at the entrance of the lacustrine part is accompanied by a further reduction of flow velocity leading to the accumulation of sediment deposits in this region. The sediment deposition surpassed the dead storage zone in the area located between 337.5 and 487 km upstream of the AHD, as clearly visible in Figs 2-7, 2-8, 2-9. Over the period 1996–2003, the water level was constantly above the elevation 175 m a.s.l., leading to sedimentation in the flood control zone. Fig 2-8 shows the sediment deposits accumulated on the both banks of the stream of the riverine part.

It should be noted that the design elevation–area–capacity curve of the reservoir adopted by MWRI was estimated by topographic maps at 1:25 000 scale. The main contour interval was 10 m, with supplementary contour intervals of 5 m between 160 and 190 m a.s.l. (Water Resources Research Institute 2007). These different methods of estimation lead to different results (Table 2).

Table 2-2 Storage capacity for different operating zones of AHDR estimated from MWRI curve and DEM

Storage zone	Data source	Year	Storage capacity (km^3)	Reduction of storage capacity (km^3)	Reduction of storage capacity (%)
Dead storage zone	MWRI	1964	31.60	6.60	11%
	DEM	2013	25.00		
Live storage zone	MWRI	1964	90.40	12.40	14%
	DEM	2013	78.00		
Flood control zone	MWRI	1964	40.00	1.00	2.5%
	DEM	2013	39.00		

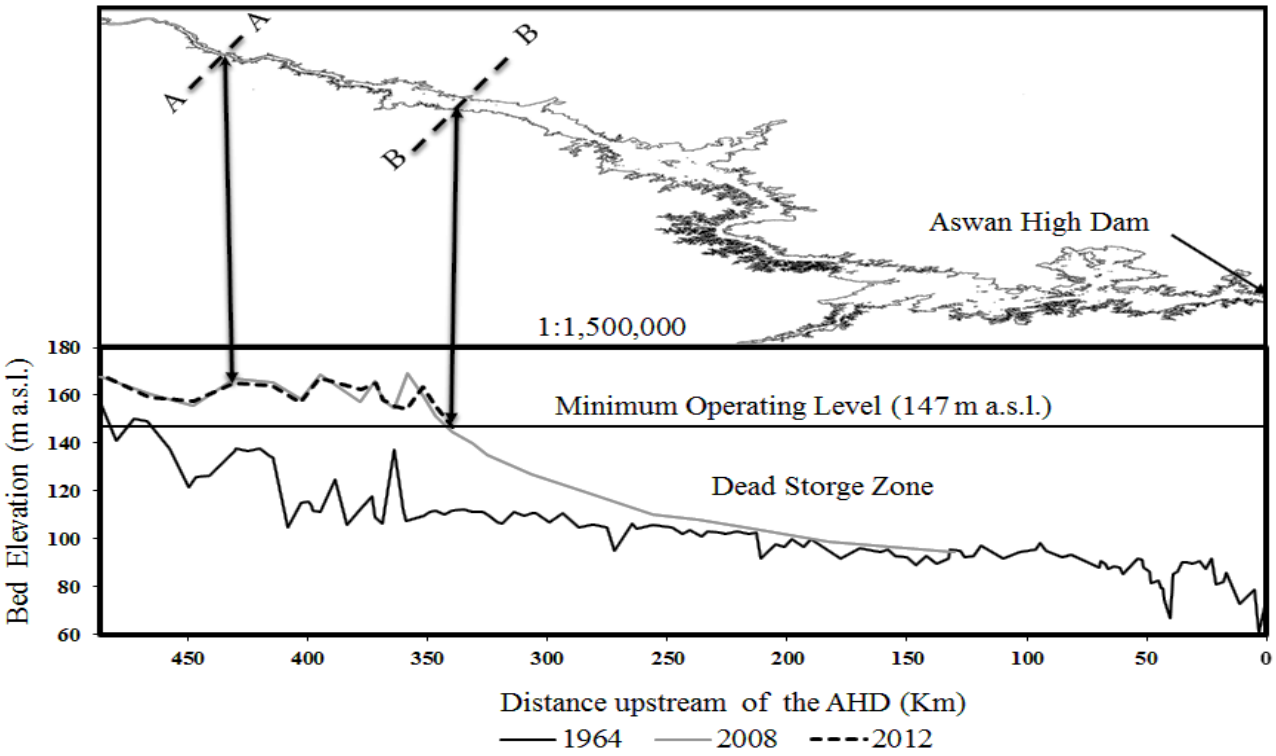

Figure 2-7 Changes in the bed elevation of the AHDR based on bathymetric survey data of years 1964, 2008 and 2012 based on data provided by MWRI

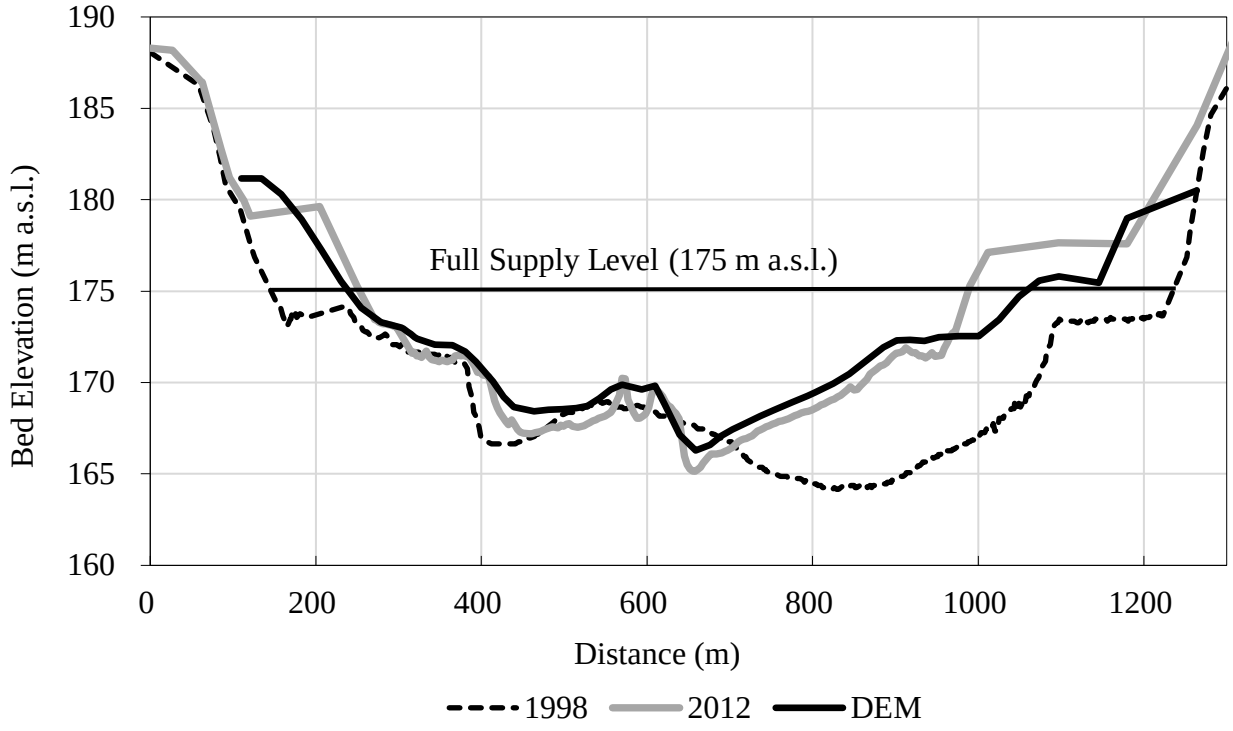

Figure 2-8 Upstream face of cross-section (A-A) at 431 km upstream of the AHD based on DEM and bathymetric survey data of years 1998 and 2012 based on data provided by MWRI

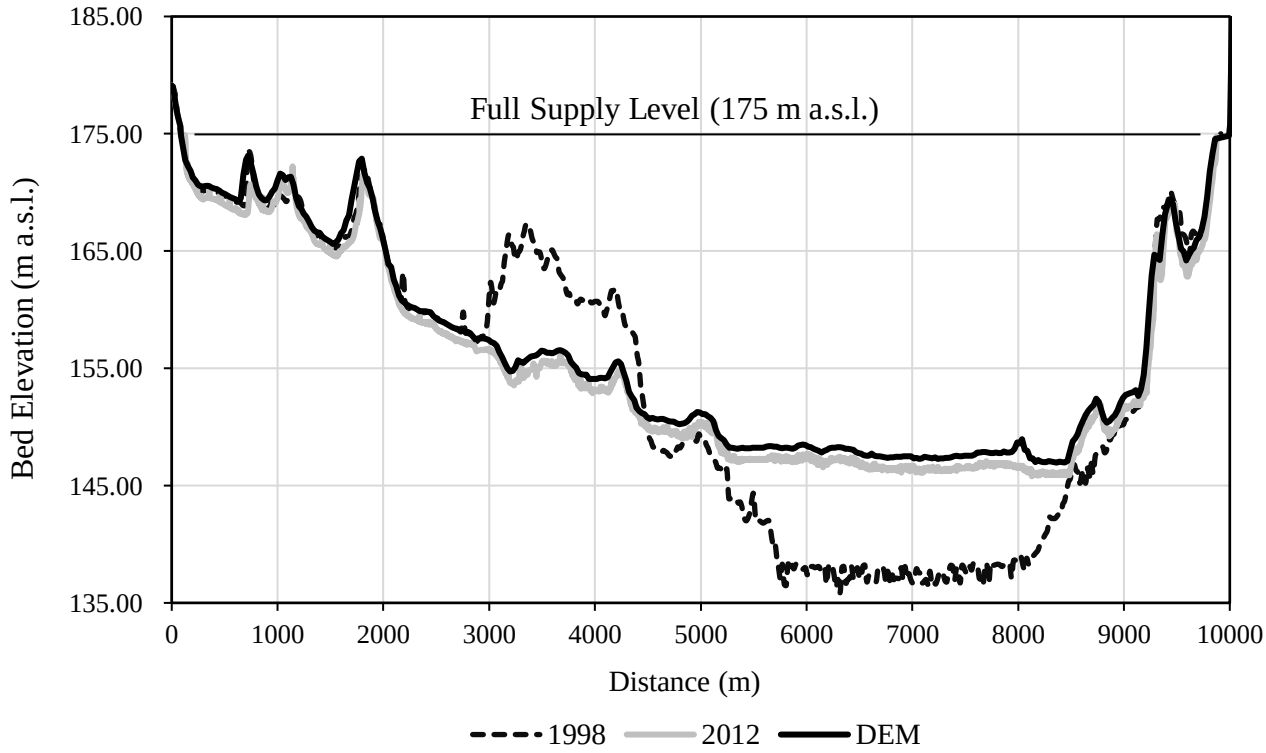

Figure 2-9 Upstream face of cross-section (B-B) at 337.5 km upstream of the AHD based on DEM and bathymetric survey data of years 1998 and 2012 based on data provided by MWRI

2.4.2 Surface Area

A comparison of the surface area curve created from the DEM, and the design curve of the AHDR is plotted in Fig 2-10. This shows that the design curve is larger than the new curve, and the differences between them increase as the water level rises, in particular between water levels of 140 and 168 m a.s.l. The average reduction of the surface area between water levels 140 and 168 m a.s.l. is about 15%. Above the water level of 168 m a. s.l. the differences between the two curves decrease with an increase in the water level. The surface area of the AHDR estimated by the DEM at the water level of 182 m a.s.l. is 6350 km^2, as shown in Fig 2-10. This value is different from the value estimated by MWRI, which is about 6540 km^2 and was estimated via 1:25 000 topographic maps.

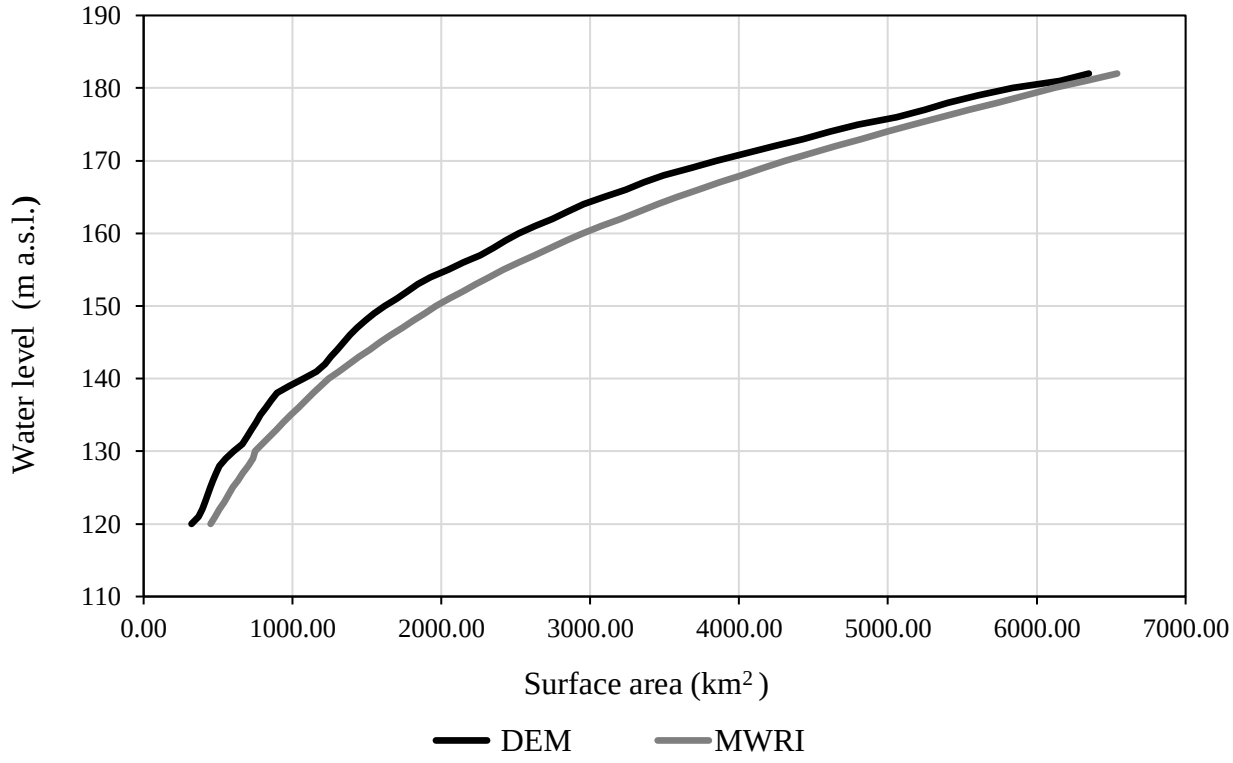

Figure 2-10 Comparison of the two surface area curves MWRI (1964) and DEM

Further, the surface area of the AHDR for the period 1987– 1990, at water levels 156.60, 161.0, 165.0 and 168.60 m a.s.l., was compared with its counterpart produced by the DEM. As shown in Fig 2-11, the area of the AHDR decreased remarkably because of sediments. The decrease in the area of the AHDR is estimated by ArcGIS software to be

7% over the last 25 years. Table 3 shows the reduction in the surface area estimated using the satellite images and the DEM.

Also, Fig 2-11(d) displays the path of the river inside the reservoir. This path gives insight into how the lacustrine part gradually changes to the riverine part and how the situation in this area is expected to progress in future years.

Table 2-3 Surface area of the reservoir estimated from MWRI curve, satellite images, and DEM

Water level (m a.s.l.)	Data source	Year	Surface area of AHDR (km^2)	Reduction of surface area (%)
156.60	MWRI	1964	2585.20	
	Satellite images	1988	2366.20	8%
	DEM	2013	2196.70	15%
161.00	MWRI	1964	3076.00	
	Satellite images	1987	2867.60	6%
	DEM	2013	2629.00	14%
165.00	MWRI	1964	3581.00	
	Satellite images	1990	3249.00	9%
	DEM	2013	3087.00	14%
168.60	MWRI	1964	4103.60	
	Satellite images	1989	3859.70	6%
	DEM	2013	3581.30	13%

The morphology of the southern part of the AHDR has changed. Via satellite images, it was possible to observe this change over relatively small time intervals. The riverine part became narrower because of sediment deposition, as shown in Fig 2-12. The morphology at the entrance of the lacustrine part under the 175 m a.s.l. level gradually converted into the riverine part as depicted in Fig 2-12(a).

Two plots of the southern part of the AHDR for 1998 and 2013, at water levels 175.24 and 175.82 m a.s.l., respectively, are superposed and presented in Fig 2-12(b). The two plots apparently match, but only the plot for 2013 shows that the sediment surpassed the 175 m a.s.l. level and is rising at the entrance of the lacustrine part. In the long run, a new delta could be formed through sediment deposition in this region.

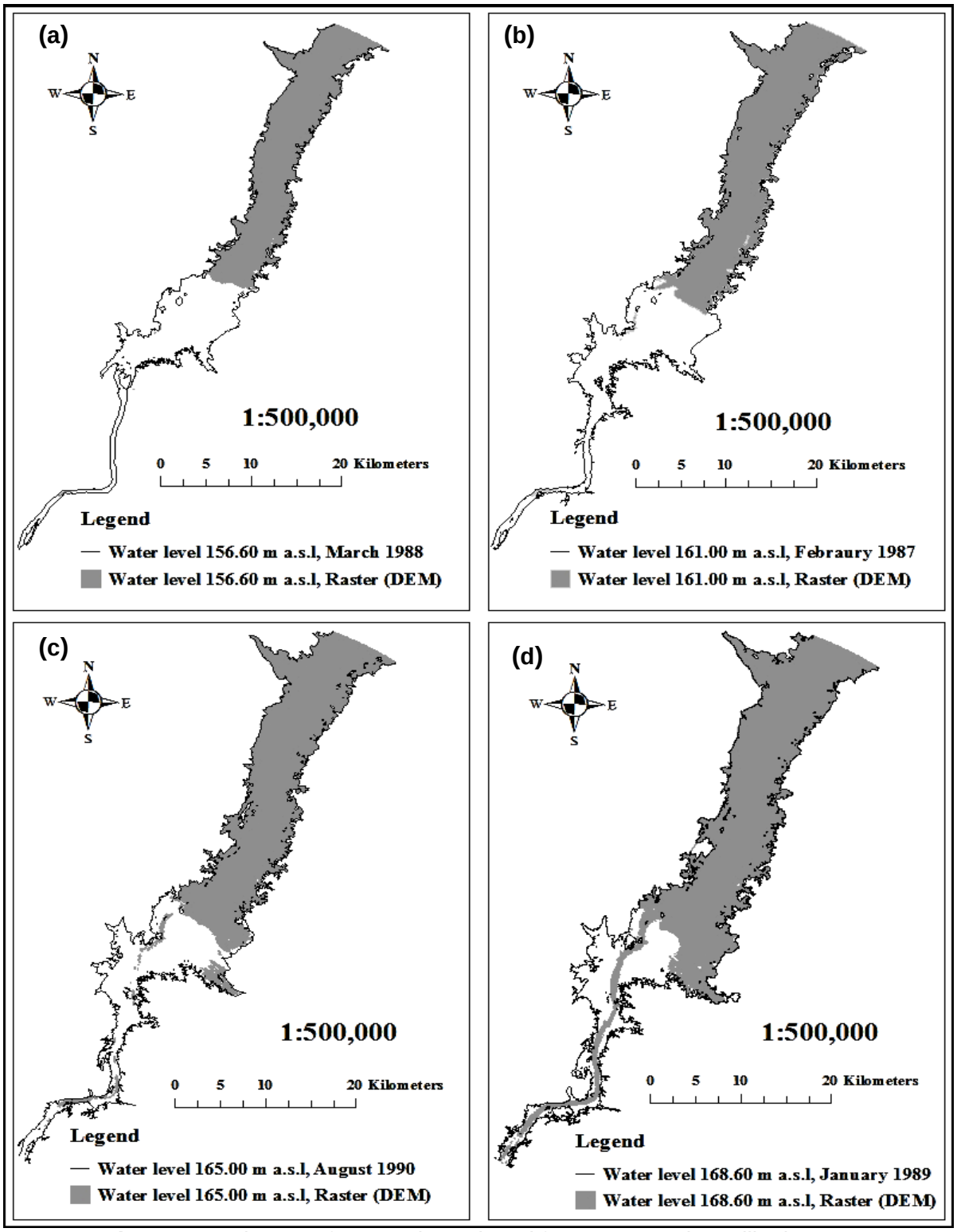

Figure 2-11 Shapes of reservoir produced from DEM and satellite image.

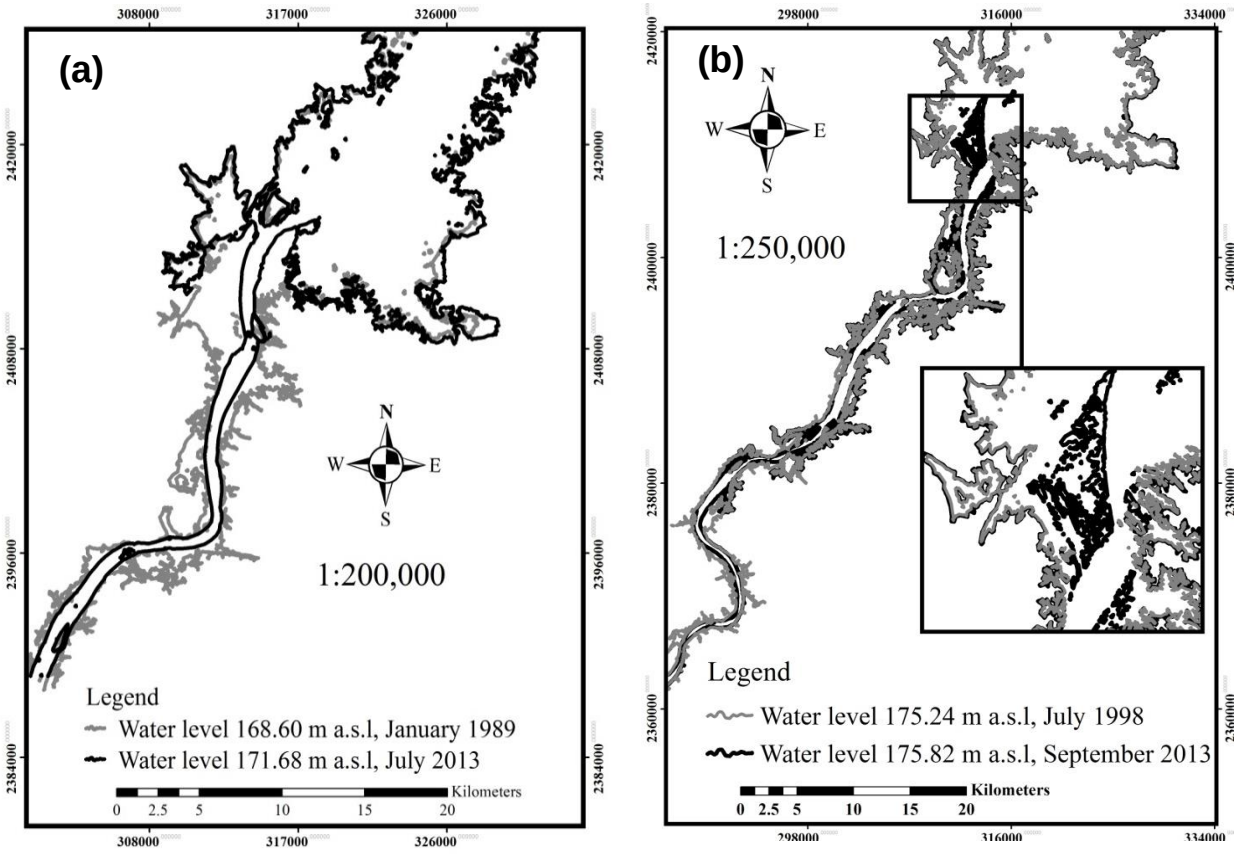

Figure 2-12 (a) Changes at the entrance of the lacustrine part of the AHDR under the level of 175 m a.s.l. for the period 1989-2013 (b) Changes at the entrance of the southern part of the AHDR above the level of 175 m a.s.l. for the period 1998-2013

2.5 Conclusions

The storage capacity of the AHDR estimated by the DEM decreased by 12% over the period 1964–2013. This reduction was mainly in the live storage capacity, the dead storage capacity, and slightly in the flood control zone. The live storage capacity, which guarantees annual water requirements, is estimated to be 78 km^3. The results show a new elevation–capacity curve for the AHDR. This new curve gives a different estimate of the water volume that flows into the reservoir and the estimated water losses using the water balance method. The new storage curve guarantees the water demands for irrigation, hydropower and water supply. The live storage capacity still meets the annual downstream requirements for water (Egypt's annual agreed quota from the Nile River is 55.5 km^3). The increase of bed elevation of the southern part of the AHDR because of sedimentation hinders navigation and hydrographic survey after flood recession.

The surface area of the AHDR decreased, particularly at the low water levels, because of sedimentation. The average reduction in the surface area between water levels 140 and 168 m a.s.l. was about 15% over the period 1964–2013, which is equivalent to almost 10 km^3. The morphology of the reservoir has changed because of sedimentation. The riverine part became narrower than before, and the entrance of the lacustrine part began to transform gradually into part of the river. Also, the sediment has surpassed the elevation of 175 m a.s.l. and is rising at the entrance of the lacustrine part.

3- Comparison of the water balance method and alternative evaporation methods applied to the High Aswan Dam Reservoir

Journal article (accepted)
Authors: El-Shazli, A., Hoermann, G., Wagner, P.D., Fohrer, N.
Journal: DIE ERDE – Journal of the Geographical Society of Berlin
Date of submission: 21 March 2017
El-Shazli, A., Hörmann, G., Wagner, P.D., Fohrer, N. (2018): Comparison of water balance method and alternative evaporation methods applied to the High Aswan Dam Reservoir. Die Erde, accepted.

3 Comparison of the water balance method and alternative evaporation methods applied to the High Aswan Dam Reservoir

Abstract:

Aswan High Dam Reservoir (AHDR) is a large human-made reservoir situated in southern Egypt and northern Sudan. The reservoir is located in a typical arid zone so that evaporation results in a significant water loss from the reservoir. To quantify these evaporation water losses, different methods can be applied. The water balance method was used to estimate water losses of the AHDR during 43 open-water seasons. Compared to earlier publications, this study used longer time series data and more evaporation approaches. Moreover, we evaluated the deviation between evaporation as derived from the water balance method and as calculated using 16 evaporation/evapotranspiration formulas. Five approaches are not well suited for use at the AHDR because they underestimated evaporation rate (e.g. Stephens-Stewart), or overestimated evaporation rate (e.g. de Bruin). Annual evaporation rate obtaind by the Bowen ratio energy balance method at the three floating stations Raft, Allagi and Abu Simbel estimated as 7.9, 6.9 and 6.7 mm d^{-1} respectivly. The monthly water losses of the years 1978 −1984, a period with reasonable evaporation rates, are used to estimate the evaporation losses. The results of the study show a systematic deviation between the monthly average values determined using the water balance method through the period 1978 –1984 and the monthly mean values determined by the 16 evaporation calculation approaches at three floating stations. This deviation is particularly clear in the months of May, June and September (primarily lower estimates) as well as in July (primarily higher estimates). The deviation can be attributed to the simplicity of the water balance method as well as to its unlikely applicability in the case of large reservoirs as the AHDR over short periods like a month. Among the 16 evaporation calculation approaches the mass transfer method provided the most reasonable results under the given site conditions.

Keywords: Aswan High Dam Reservoir (AHDR); Water balance method; Evaporation; Methods comparison

3.1 Introduction

Water storage in reservoirs is one of the mechanisms for dealing with the fluctuation of water supply and demand (Wisser *et al.*, 2013). Constructing large surface reservoirs can be used to increase the water resources during the low flow limiting periods and drought seasons (Shiklomanov, 1998). The main uses of surface water reservoirs include flood control, municipal water supply, power generation, irrigation, commercial and recreational fisheries and navigation. About 70% of the rivers around the world are obstructed by large reservoirs (Nilsson *et al.*, 2005).

The loss of water from reservoirs is a great challenge in water-scarce and arid areas, in particular, the evaporation losses. In dry areas, the evaporation losses from reservoirs can be astounding (Goldsmith and Hildyard 1986). Reservoirs can be considered one of the greatest freshwater consumers because they lose too much water by evaporation in water-scarce regions, leading to a lack of water resources (Shiklomanov, 1998). Evaporation is the major loss from the system but, contrary to losses by infiltration, the evaporative loss does not have any direct benefits to the environment of the reservoir (Abbasi and Giesen 2012).

Before erecting the Aswan High Dam (AHD), the water losses from the AHDR were estimated at 10 km^3 yearly, of which 9 km^3 were evaporation losses. The average seepage losses were rationally estimated at 1 $km^3\ yr^{-1}$ (Wafa and Labib 2000). For many years, The Ministry of Water Resources and Irrigation (MWRI) in Egypt adopted the evaporation value 7.54 mm d^{-1}, a depth of 2.7 meters, as the mean annual evaporation value from the reservoir surface. The maximum and minimum values were estimated in June and December as 10.80 mm d^{-1} and 3.95 mm d^{-1} respectively (Whittington and Guariso 1983). Afifi and Osman (1993) estimated the annual evaporation losses during the period from 1964/1965 to 1990/1991 as 9.6 km^3. Afifi and Osman (1993) used half the value of Piche evaporimeter observations, estimated by Hurst and Black in 1955, and corresponding monthly water surface areas of reservoir obtained from the area survey maps. Sadek *et al*. (1997) depended on limited data collected from ground stations erected around the AHDR. They used five different methods: water balance,

energy balance, Dalton, Penman and Complementary Relations Lake Evaporation (CRLE) model (Morton), to estimates the evaporation losses from the AHDR. Research results indicate that the minimum average annual evaporation was 5.7 mm d^{-1} for CRLE, and the maximum estimate was 7.1 mm d^{-1} for Dalton. The average annual evaporation for all approaches, after excludeding the Dalton method, because it provided high evaporation values, is 6.0±0.3 mm d^{-1}. Omar and El-Bakry (1981) used meteorological data collected during expeditions to the AHDR over the years 1970–1971. The authors estimated the evaporation rates by the bulk aerodynamic and energy budget methods. They estimated the average annual evaporation as 7.4 mm d^{-1} with a maximum evaporation rate of 10.9 mm d^{-1} in June and minimum evaporation rate of 3.8 mm d^{-1} in January. Elsawwaf *et al.* (2010a) compared the evaporation rates obtained by six evaporation approaches with the rates determined using the Bowen ratio energy budget method (BREB). The used data were obtained from three hydro-meteorological stations deployed on the AHDR over the period 1995–2004 to update the previous evaporation estimates. Research findings indicate that the evaporation rates are in the range of 2.5 to 11.2 mm d^{-1} with an average evaporation rate of 5.9 mm d^{-1}.

For the Doosti dam reservoir in Iran, Majidi *et al.* (2015) used limited data to test and rank eighteen evaporation methods based on the BREB method to determine the most appropriate evaporation methods. The result of the study showed that The Jensen-Haise, Makkink, Penman and de Bruin methods were among the most consistent methods with BREB. They concluded that methods which rely only on air temperature, or air temperature combined with day length data were practical options for estimating the evaporation rates in the study area because of their simplicity, low sensitivity, and high accuracy.

While these studies provide different values for the estimation of evaporation, a systematic comparison and evaluation of methods, in particular, water balance method, are still missing.

Therefore, the objectives of this study are: (1) to determine the water losses from the AHDR using the water balance method; (2) to determine the evaporation rate from the AHDR using 16 alternative evaporation/evapotranspiration methods; and (3) to measure the deviation between evaporation rates determined by the

evaporation/evapotranspiration methods and the evaporation rate estimated by the water balance method.

3.2 Materials and Methods

AHDR is a large surface water reservoir that is located in southern Egypt, and northern Sudan and extends between latitudes 20˚27' to 23˚58' N and longitudes 30˚35' to 33˚15' E (Entz, 1976). AHDR was formed by constructing the AHD across the Nile River at Aswan in 1960. The AHDR is situated in a hyper-arid area. Precipitation is extremely scarce in the AHDR area. The mean wind speed over the year is in the range of 4.2 to 5.3 m s^{-1} (15 to 19 km h^{-1}), and its direction is NW-NE (Elshemy, 2010). The mean slope of the mountainous eastern shoreline of the AHDR is steeper than the flat and wide western one (El Shahat, 2000). The storage capacity of the AHDR at maximum water level (182 m a.s.l.) was estimated as 162.3 km^3, with an area of 6540 km^2. The length of the AHDR at maximum level is about 500 km, partitioned into Nasser Lake in Egypt (350 km), and Nubia Lake (150 km) in Sudan, with an average width of 12 km (Elshemy, 2010).

Hydrological data of the AHDR as water volume arriving the south mouse of AHDR, water elevation of the AHDR, and water volume arriving the AHD for the period 1968 to 2011 was used to estimate the water losses with the water balance method.

The meteorological data are obtained from three floating stations distributed along the reservoir as shown in Fig. 3 -1. These stations are: Raft (2 km upstream of the AHD); Allaqi (75 km upstream of the AHD); and Abu Simbel (280 km upstream of the AHD). The three stations provided measurements of air temperature, relative humidity, lake temperature, wind speed (depicted in Fig. 3-2), wind direction, net radiation, barometric (atmospheric) pressure, and temperature–depth reservoir water profile. The available time series data of Raft station represent the period from January 1995 to December 2011, of Allaqi station from February 1995 to October 2011, and of Abu Simbel station from January 1999 to December 2011. The total period of missing data at Abu Simbel station is 14 months distributed over the years 1999, 2005 and 2009. The amount of missing data at the Raft station is less than 11 months distributed over many years. The amount of missing data at Allaqi is the biggest among the stations. The total period is about 30 months distributed over the years 1995 to 2000 and 2008 to 2010.

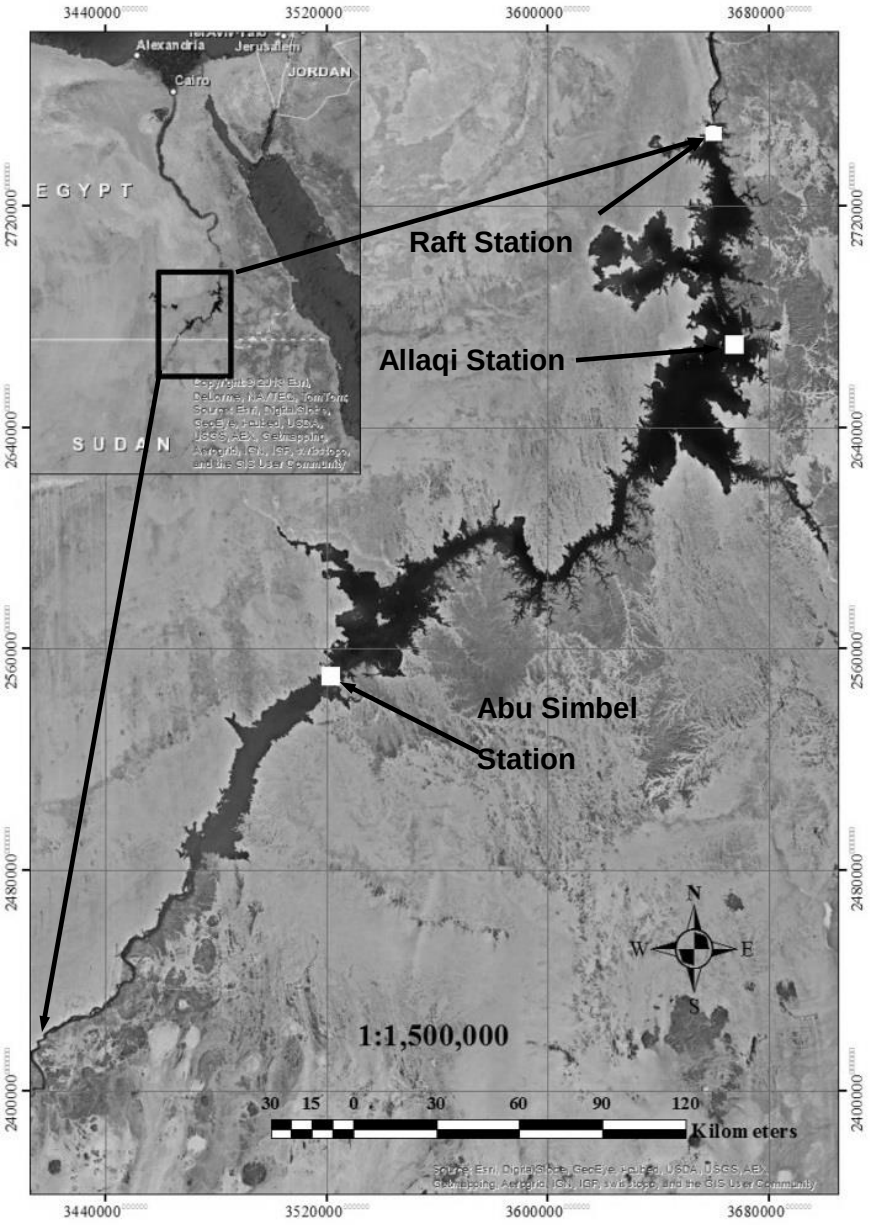

Figure 3-1 Location map of the reservoir and the Floating stations

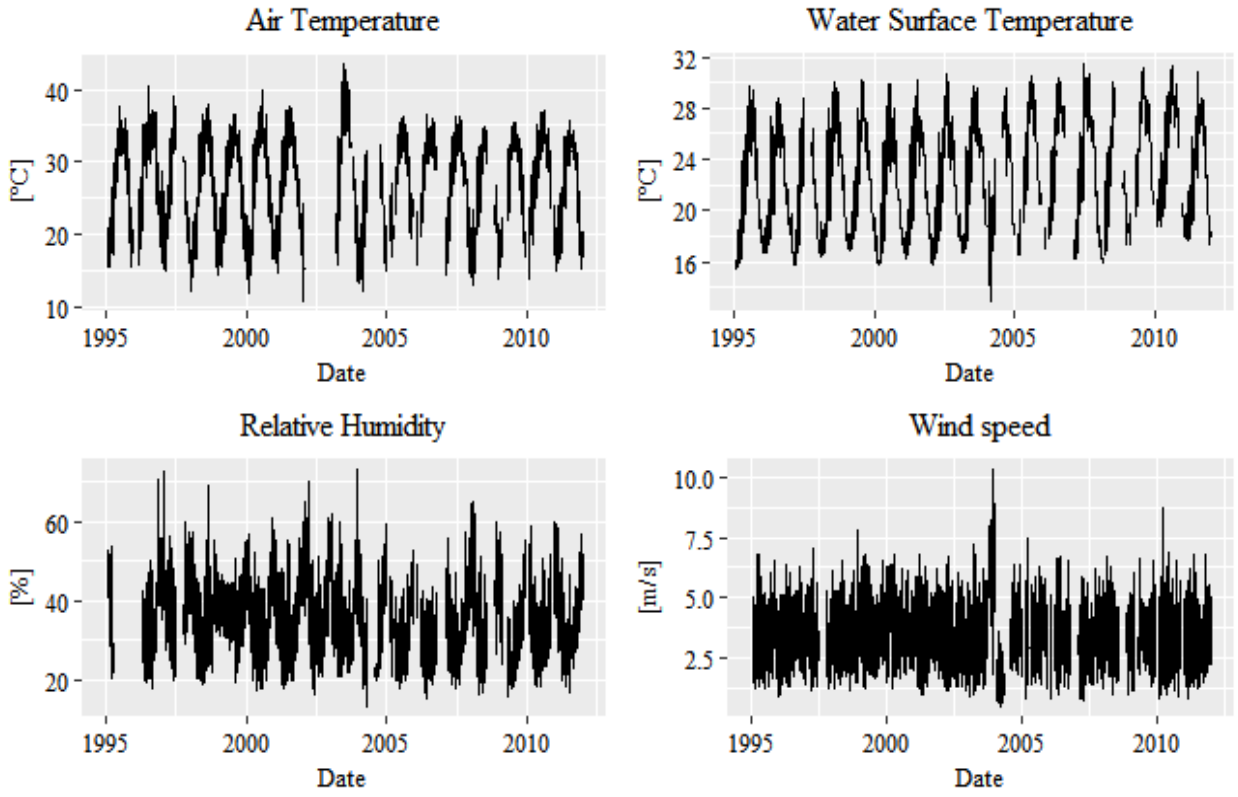

Figure 3-2 Time series of daily climate data from Raft station

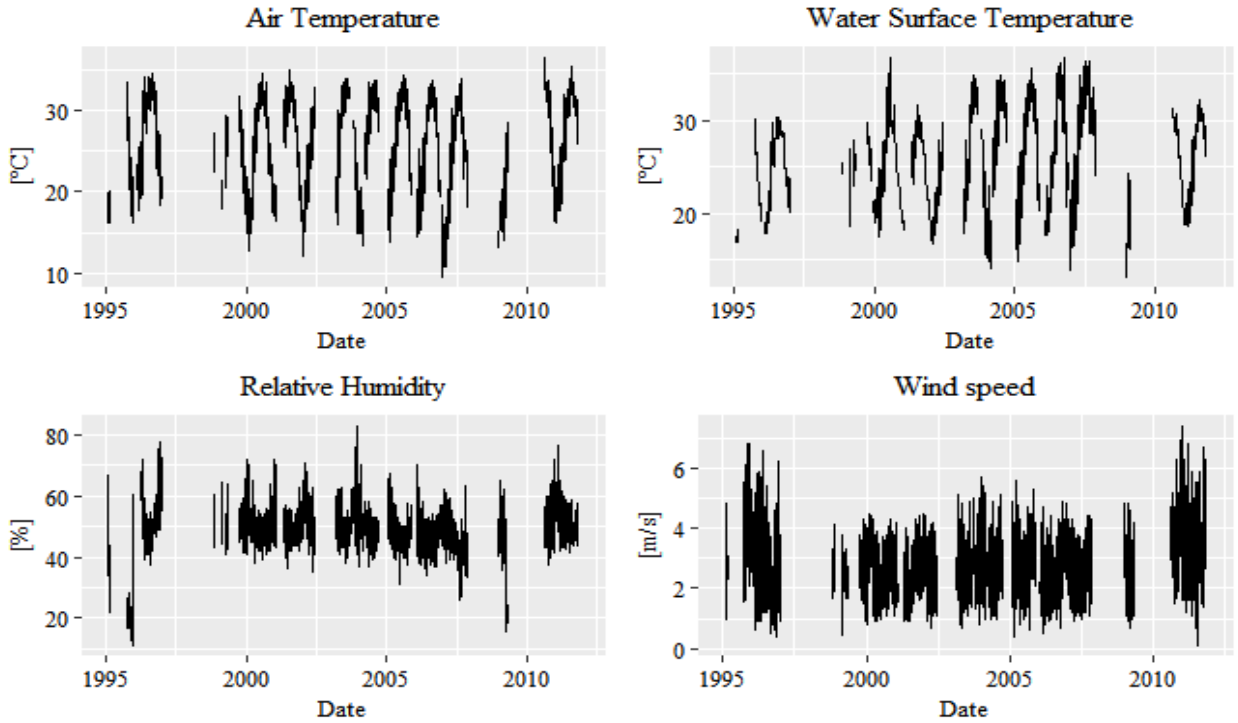

Figure 3-3 Time series of daily climate data from Allaqi station

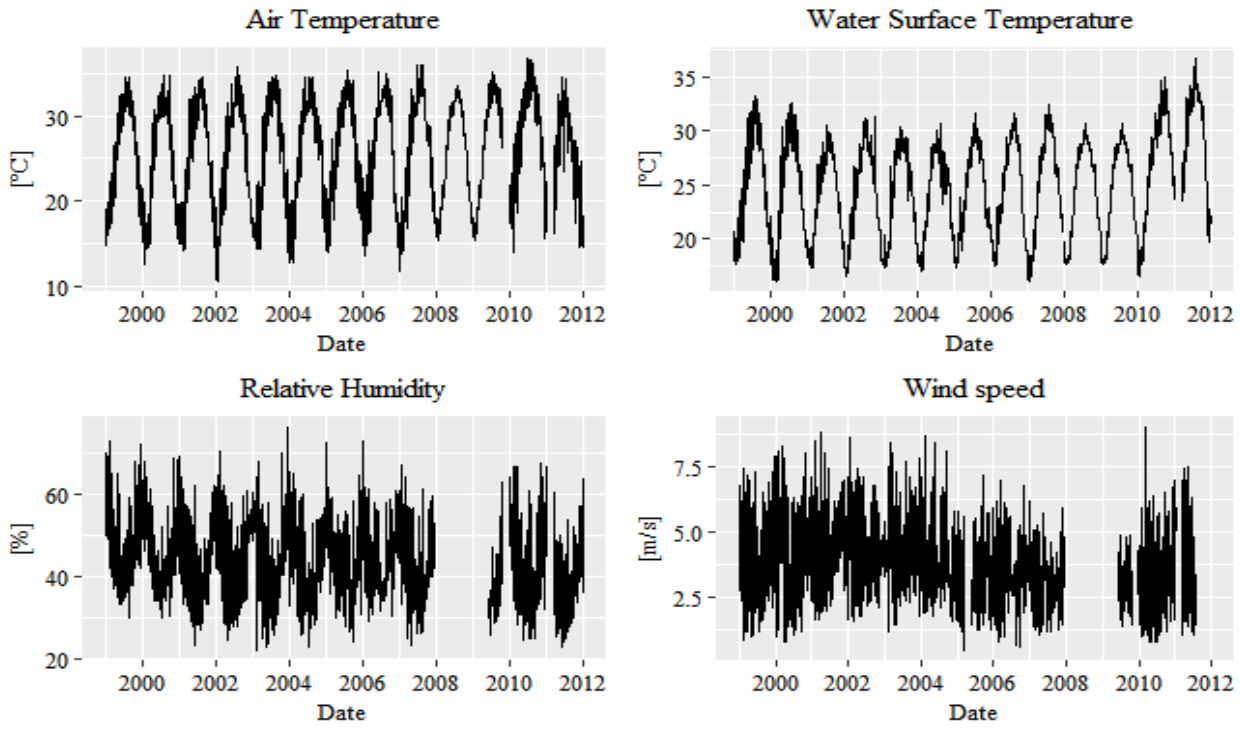

Figure 3-4 Meteorological time series data at the Abu Simbel station

3.2.1 Water Balance Method

The water balance method is a simple method to determine the water losses over a specified period. The water balance equation seems deceptively simple; water inflow equals water outflow, plus or minus the change in storage (Winter, 1981).

The water balance equation can be expressed regarding the volume of water losses per unit time as:

$$Q_1 - L - Q_A + P \pm \Delta S = 0 \quad (1)$$

where:

$$Q_1 = Q_d - Q_{S,L} \quad (2)$$

$$Q_A = Q_{D,S} + Q_T \quad (3)$$

$$\Delta S = S_2 - S_1 \quad (4)$$

Q_1 is the inflow discharge calculated at the entrance of the reservoir. L is the total actual losses from the reservoir. Q_A is the water volume arriving at the AHD. P is the precipitation on the water surface of the AHDR. ΔS is the change in storage content during the time interval (month in this study). S_2 and S_1 are the water volume of the reservoir at the end and at the beginning of the time interval. Q_d is the discharge

measured at Dongola gauging station, which is located 780 km upstream AHD (Fig. 3-5). $Q_{S,L}$ is estimated as 1% of the discharge measured at Dongola and representing Sudan abstract in the reach between Dongola and entrance of the reservoir in addition to the transmission water losses in this reach. This percentage does not remain constant. The Ministry of Irrigation and Water Resources in Egypt estimated the transmission water losses in the reach between Dongola and entrance of the reservoir as 0.3%, and downriver the value is approximately 1% due to irrigation demands in this reach. Also, Sadek et al. (1997) estimated a 1% loss of the Dongola station discharge. $Q_{D.S}$ is the outflow discharge downstream AHD. Q_T is the outflow discharge through Tushka spillway at 270 km upstream the AHD (if any). The main annual rainfall on the AHDR area is less than 10 mm yr^{-1} (Shahin, 1985). Therefore, the above equation can be re-written as:

$$Q_1 - L - Q_A \pm \Delta S = 0 \qquad (5)$$

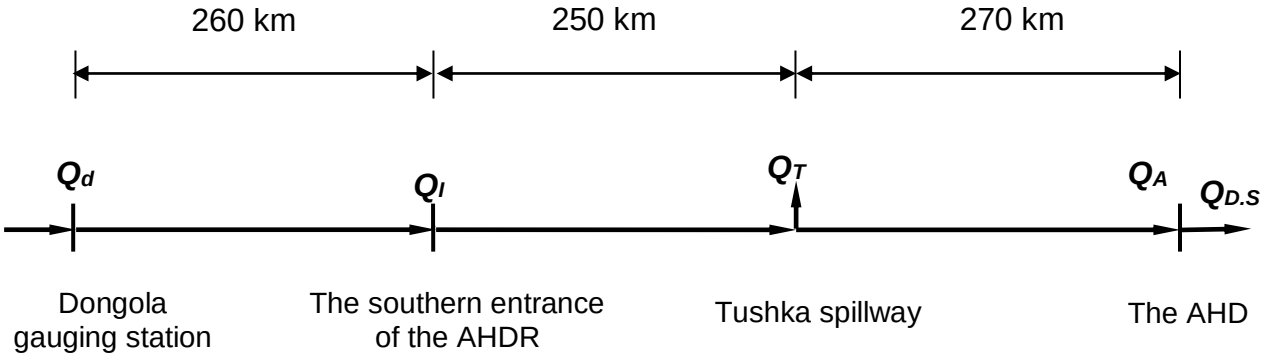

Figure 3-5 Water flows into and out of the AHDR

The hydrological data for 43 years, from the water year (August to July) 1968/1969 to the water year 2010/2011, is used to estimate the water losses from AHDR by the water balance method. The monthly values of the water volume measured at Dongola gauge station, the water volume arriving upstream AHD and the change of water volume of AHDR are used to estimate the monthly water losses.

3.2.2 Evaporation Methods

Several evaporation models were selected to determine the evaporation values in the AHDR using meteorological data collected at three floating stations. Some of these

evaporation models are mainly used for terrestrial sites, but they can also be used for lakes (Rosenberry *et al.* 2007; Elsawwaf *et al*.2010a, 2010b; Majidi *et al.* 2015). The evaporation methods are grouped, as depicted in Table 1, into six groups, i.e.: (i) the energy balance, (ii) the combination, (iii) the solar radiation-temperature, (iv) the Dalton, (v) the temperature and (vi) the temperature- day length.

Table 3-1 Methods for estimation of evaporation rate (E)

Method	Reference	Equation
Energy budget		
BREB	Harbeck et al., (1958)	$E = \frac{Q_n + Q_v - Q_x}{\rho_w\left(L(1+BR) + c_w(T_0 - T_b)\right)} \times 86.4 \times 10^6$
Combination group		
Priestley–Taylor	Priestly and Taylor (1972)	$E = \alpha(\frac{\Delta}{\Delta+\gamma})\left[\frac{Q_n - Q_x}{L\,\rho_w}\right] \times 86.4 \times 10^6$
deBruin–Keijman	De Bruin and Keijman (1979)	$E = (\frac{\Delta}{0.85\Delta + 0.63\gamma})\left[\frac{Q_n - Q_x}{L\,\rho_w}\right] \times 86.4 \times 10^6$
Penman	Brutsaert (1982)	$E = (\frac{\Delta}{\Delta+\gamma})\left[\frac{Q_n - Q_x}{L\rho_w}\right] \times 86.4 \times 10^6 + (\frac{\gamma}{\Delta+\gamma}) \times [0.26(0.5 + 0.54U_2)(e_s - e_a) \times 10^{-2}]$
Brutsaert–Stricker	Brutsaert and Stricker (1979)	$E = (2\alpha - 1)(\frac{\Delta}{\Delta+\gamma})\left[\frac{Q_n - Q_x}{L\rho_w}\right] \times 86.4 \times 10^6 - (\frac{\gamma}{\Delta+\gamma}) \times \left[0.26\,(0.5 + 0.54U_2)(e_s - e_a) \times 10^{-2}\right]$
deBruin	(De Bruin, 1982)	$E = 1.192\left(\frac{\alpha}{1-\alpha}\right)\left(\frac{\gamma}{\Delta+\gamma}\right)\left[\frac{(2.9 + 2.1U_2)(e_s - e_a) \times 10^{-2}}{L\,\rho_w}\right] \times 86.4 \times 10^6$
Solar radiation, temperature group		
Jensen–Haise	(Ward and Trimble, 2003)	$E = \frac{C_T\,(T_a - T_x) \times Q_s}{11.6 \times L} \times 10^6$
Makkink	Delclauxet al., (2007)	$E = a_1(\frac{\Delta}{\Delta+\gamma})\left[\frac{Q_s}{L\rho_w}\right] \times 86.4 \times 10^6 + b_1$
Stephens–Stewart	Elsawwaf et al., (2010 b)	$E = \left(a_2\left(\frac{9 \times T_a}{5} + 32\right) + b_2 \times (Q_s \times 3.495 \times 10^{-2})\right)$
Hargreaves	Xu and Singh (2000)	$E = a_3(T_a + b_3)\left[\frac{Q_s}{L\rho_w}\right] \times 86.4 \times 10^6$
Dalton group		
Mass transfer	Harbeck et al., (1958)	$E = NU_2(e_0 - e_a) \times 86.4 \times 10^6$
Ryan–Harleman	Rasmussen et al., (1995)	$E = \frac{(2.7(T_0 - T_a)^{0.333} + 3.1U_2)(e_0 - e_a) \times 10^{-2}}{L\,\rho_w} \times 86.4 \times 10^6$
Temperature group		
Papadakis	Rosenberry et al., (2007)	$E = 0.5625\left(e_s\,max \times 10^{-2} - (e_s\,min \times 10^{-2} - 2)\right)\left(\frac{10}{d}\right)$
Thornthwaite	Watson (1993)	$E = \left(1.6\left(\frac{10T_a}{I}\right)^{6.75\times10^{-7}I^3 - 7.71\times10^{-5}I^2 + 1.79\times10^{-2}I + 0.49}\right)\left(\frac{10}{d}\right)$

Temperature, day length group

Blaney–Criddle	Rosenberry et al., (2007)	$\mathrm{E} = (0.0173\mathrm{T_a} - 0.314) \times \mathrm{T_a} \times \left(\frac{\mathrm{D}}{\mathrm{D_{TA}}}\right) \times 25.4$
Hamon	Rao et al., (2011)	$\mathrm{E} = 0.1651 \times L_{day} \times \rho_{sat}$

where Q_n net radiation (W m^{-2}); Q_v net advective energy (Wm^{-2}); Q_x change in thermal energy storage (W m^{-2}); BR, Bowen ratio, dimensionless; T_o lake surface temperature (^{o}C; ^{o}F for the Blaney–Criddle equation); ρ_w density of evaporating water (998 kg m^{-3}); L Latent heat of vaporization (J kg^{-1}); c_w specific heat capacity of water (4186 J kg^{-1} K^{-1}); T_b reference base temperature (assume 0 ^{o}C); α = 1.26, Priestley–Taylor constant, dimensionless; Δ slope vapor pressure curve (Pa K^{-1}); γ psychometric constant (Pa K^{-1}); e_s saturated vapor pressure at temperature of the air (Pa); e_a vapor pressure at 2 m above the water surface (Pa); e_o saturation vapor pressure at the water–surface temperature (Pa); e_s max and e_s min = saturated vapor pressures at daily maximum and minimum air temperatures (Pa); N coefficient of efficiency of vertical transport of water vapor by eddies driven by the wind ($N = \frac{0.622\rho_a}{P_a\rho_w}\frac{0.16}{\left[ln\left(\frac{Z_m - Z_d}{Z_o}\right)\right]^2}$) (Pa^{-1}), ρ_a density of air [1.220 kg m^{-3}], Z_m height at which wind speed and air vapor pressure are measured; Z_d zero−plane displacement [m], Z_d=0 over typical water surfaces, Z_o roughness height of the surface [m], Z_o=2.30×10^{-4} m over typical water surfaces; T_a air temperature at 2 m above the AHDR surface (^{o}C); U_2 wind speed at 2 m above AHDR surface (m s^{-1}); d number of days in the month; I annual heat index ($I = \Sigma\ i$, $i = (T_a/5)^{1.514}$); D hours of daylight; D_{TA} total annual hours of daylight for specific latitude; Q_s solar radiation (W m^{-2}); T_x intercept of the temperature axis (T_x = − 2.5 − 1.4 ×10^{-3}(e_s max − e_s min) − H/550) (^{o}C); C_T temperature coefficient ($C_T = \frac{1}{C_1 + 7.3C_H}$); $C_1 = 38 - \frac{2H}{305}$; $C_H = \frac{5.0\ kPa}{e_s max - e_s min}$, H the water level of AHDR (m); L_{day} daytime length; ρ_{sat} saturated vapour density (g m^{-3})$\left(\rho_{sat} = \frac{216.7 \times e_s \times 10^2}{T + 273.3}\right)$; a_1=0.77, a_2=0.008, a_3=0.0145,b_1=0.2, b_2=−0.19, b_3=17.8; the multipliers 10, 10^{-2}, 25.4, and 86.4 $\times 10^6$ are conversion factors to mm d^{-1}.

Q_n values were identified according to the FAO-56 procedure (Allen et al. 1998). Q_x was computed from the daily temperature profile of the water body at depths 0, 2, 5, 10, 15, and 20 m. The formula for the change in heat storage in the water body (Q_x) can be expressed as:

$$Q_x = \rho_w c_w \left(0.5 \sum_{i=1}^{5} [\Delta t_i + \Delta t_{i+1}] \Delta z_i\right) \quad (6)$$

where Δt_i , $\Delta\ t_{i+1}$ are water temperature differences between two timepoints of one day, frequently measured at two depths. Δz_i is the layer thickness (depth zone).The output values of Eq. 5 were multiplied by 11.574×10^{-6} to convert the unit of Q_x to W m^{-2}.

The monthly Q_x values of the three hydrometeorological stations are shown in Fig. 3-6. The net decrease or increase in Q_x equals −0.43, −24.6 and 1.2 W m^{-2} through the whole period at Raft, Allaqi, and Abu Simbel stations, respectively. These values should be close to zero, which only applies to Raft and Abu Simbel. The stored heat in reservoirs is mainly governed by the surface energy exchanges rather than the energy

exchanges at the water-soil interface and the energies associated with the inflows and outflows (Henderson-Sellers, 1986). Therefore, the Q_v term (net advective energy by groundwater, precipitation, and stream flow) can often be neglected if the reservoir water volume is large compared to the water volumes flowing in and out of the reservoir or if the temperature values are convergent (Finch and Calver 2008).

BR is the ratio of sensible heat to latent heat and is calculated as:

$$BR = \frac{c_{pa} P_a}{0.622 L} \frac{T_0 - T_a}{e_0 - e_a} \quad (7)$$

where c_{pa} is the specific heat capacity of moist air at constant pressure (1.01 kJ kg^{-1} K^{-1}).

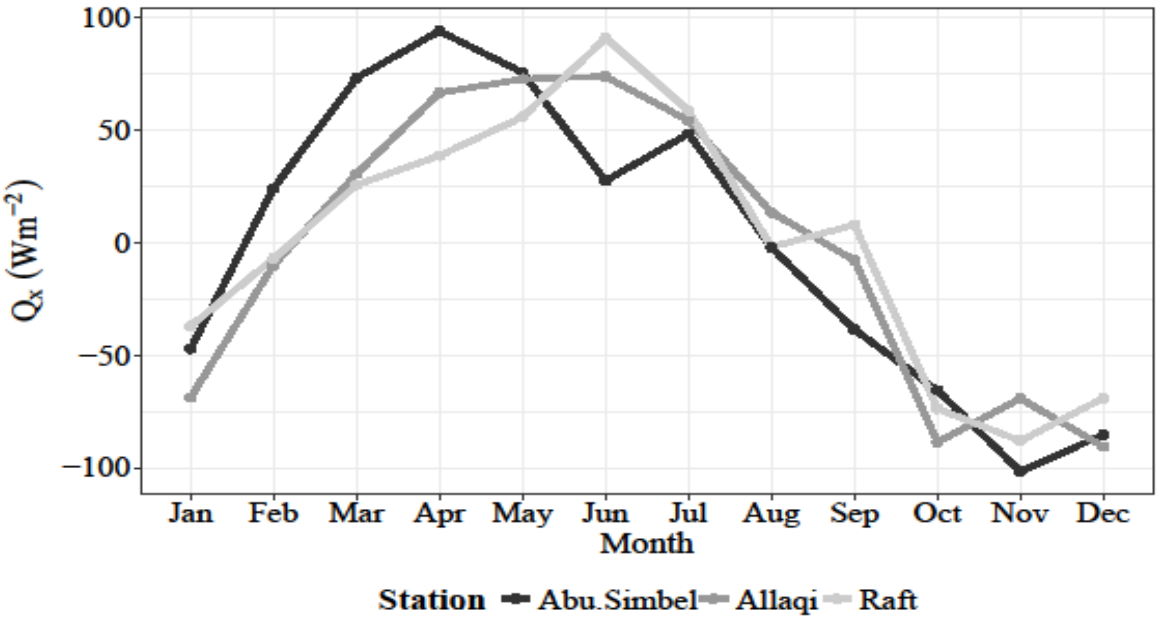

Figure 3-6 Change in heat content at all hydrometeorological stations determined by Eq. 5

3.3 Results and Discussion

3.3.1 Water Balance Method

The total annual water losses during the period from 1968/1969 to 2010/2011 amounted to 413 km^3, giving an average annual value of 9.6 km^3 yr^{-1}. This means that the annual average water loss is close to the designed value (10 km^3 yr^{-1}). However, there has been some unusual variance in water loss at this period as depicted in Fig.3-7. The monthly evaporation rates of the periods 1968–2011, 1995–2011 and 1978–1984 are used to approximate the evaporation losses as depicted in Fig. 3-8. The evaporation

rates of the periods 1968–2011 and 1978–1984 are relatively similar. However, the period 1978–1984 has two advantages: Firstly, there has not been unusual variance in water loss in this period. And secondly, the water elevation started to decrease during this period and this means there is no loss by absorption (loss because of saturation of dry rock). Also, the seepage water loss is expected to be lower. In general, the seepage loss is very low and can be neglected (estimated as 0.24 km^3 yr^{-1} (Aziz et al., 2014)). The uncertainty of the discharge measurements at Dongola station which required to determine the limits of water balance method is unknown.

The average annual evaporation rate was estimated, during the period 1978–1984, as 5.5 mm d^{-1} with a maximum in July (10.1 mm d^{-1}) and a minimum in February (3.3 mm d^{-1}). The evaporation in July and August is about two times the other values (Fig. 3-8).

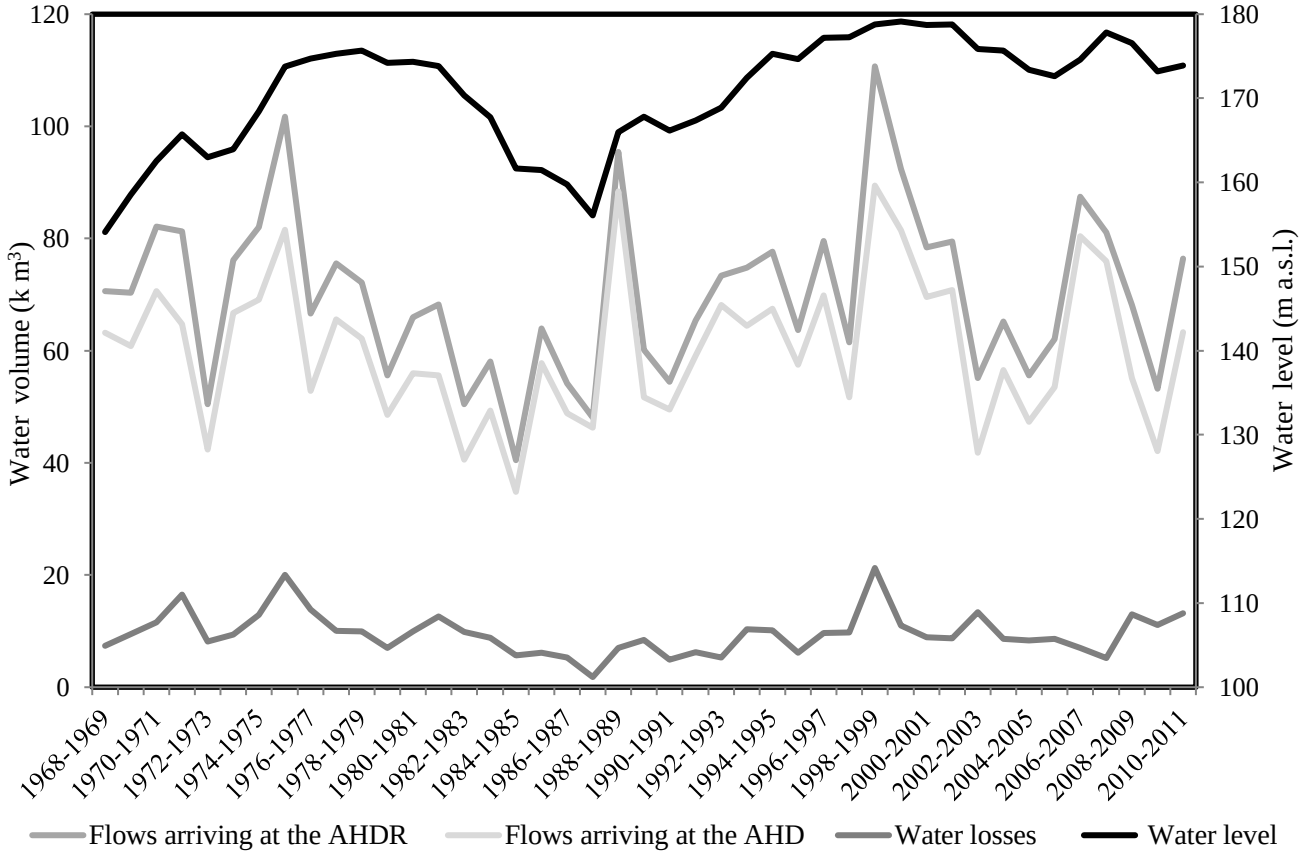

Figure 3-7 Annual water losses as derived by the water balance method, depicted with the flows arriving at the AHDR, flows arriving at the AHD, and average water level.

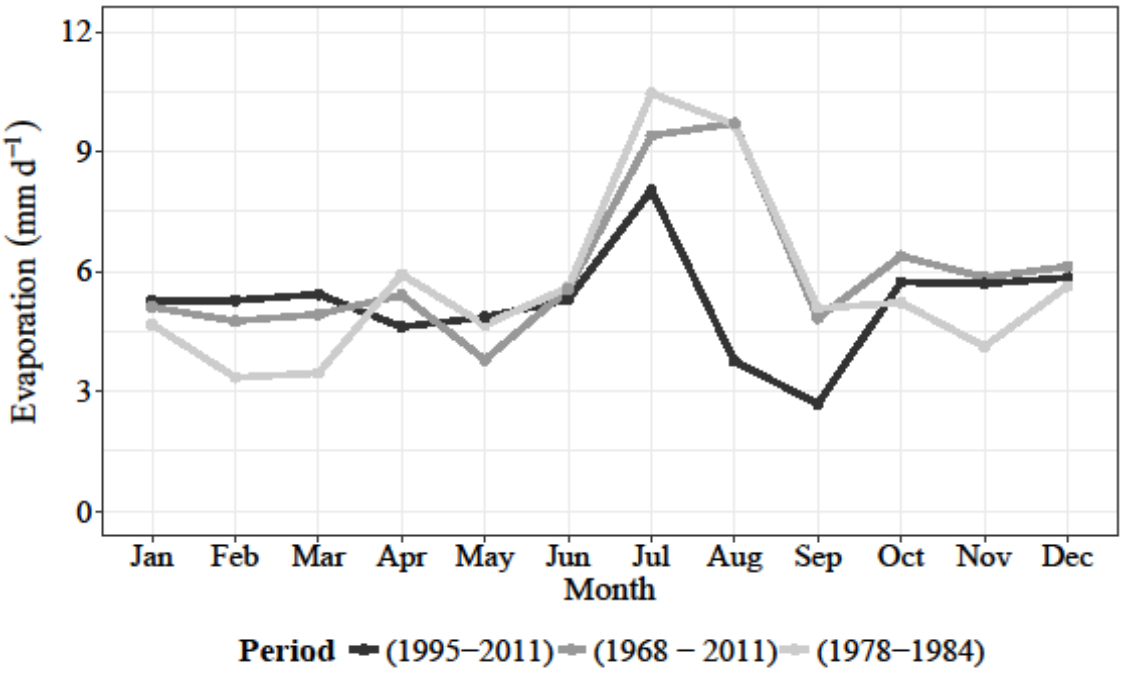

Figure 3-8 Monthly average evaporation values in mmd^{-1} from AHDR as calculated by water balance method

3.3.2 Alternative evaporation methods

3.3.2.1 The Bowen Ration Energy Balance (BREB) method:

In this method, the evaporation from a water body is determined as the energy term required to close the energy budget when all the other terms of the budget of the water body are known. If the sensible heat flux term (the amount of energy directly warming the air) is not measured directly, then it can be replaced by the Bowen ratio (BR, defined as the ratio between the sensible and latent heat fluxes) in the energy balance equation (Finch and Calver 2008). As depicted in Table 2, the BR at Raft station are more negative than the values at Allaqi and Abu Simbel stations. It is explained by the higher negative values of the (T_0-T_a). The value of evaporation rate loses its numerical meaning when the Bowen ratio approaches −1.0 (Ohmura, 1982), as occurred at Raft station.

As depicted in Fig. 3-9, the BREB determined highest evaporation rates at Raft station because of the high negative values of BR. The evaporation rates, as well as the BR values, at Allaqi and Abu Simbel station, are very similar. In general, the BREB is a very sensitive method and requires high-quality data to get a good result over open water surfaces.

3.3.2.2 Combination group

Combination methods include available-energy and aerodynamic terms. Penman combined the mass transfer and energy budget methods and excluded the requirement for surface temperature to get his equation for the evaporation rate from open water (Majidi *et al.* 2015). Priestley-Taylor neglected the aerodynamic term in Penman's equation and used a constant α (as correction factor) with the energy component. Priestley and Taylor estimated the average value of α at 1.26. De Bruin-Keijman derived their equation based on the Priestley-Taylor equation. They replaced the term of $\alpha(\Delta/(\Delta+\gamma))$ by the term of $(\Delta/(0.85\Delta+0.63\gamma))$ because they found diurnal variation in the value of α and suggested that the conditions producing such variation would be expected from many lakes. Also, they found a very good agreement between the evaporation determined from the energy budget and that determined using their Formula (Finch and Calver 2008). Brutsaert-Stricker formulated Advection-Aridity (AA) model using a simple, empirically based, linear approximation for the wind function proposed by Penman (1948) and substituting this approximation into the Penman equation. They also used the Priestley and Taylor equation for partial equilibrium evaporation (Hobbins et al., 2001). De Bruin found that it is often not possible or too expensive to get satisfactory measurements of Q_n and Q_x for a large water body. Thus, he combined the Penman and Priestley-Taylor equations and excluded the energy components (Finch and Calver 2008). As depicted in Fig. 3-9, the evaporation rate at the three floating station determined by Priestley-Taylor and de Bruin-Keijman approaches are very similar. Penman determined relatively high evaporation rate compared to Priestley-Taylor and de Bruin-Keijman approaches, while de Bruin overestimated the evaporation rate. Evaporation rates determined by Brutsaert- Stricker at Raft station are very low and not realistic for the site's climate conditions.

3.3.2.3 Solar radiation, temperature group

The evaporation rate determined by the four temperature-radiation methods increases when the value of Q_S and T_a increases. This explains the high evaporation rate in July and August. The coefficients used in these methods emphasize the influence of Q_S and T_a to some extents (Rosenberry et al., 2007). The evaporation rate estimated by Hargreaves and Makkink are convergent. Stephens-Stewart and Jensen–Haise

approaches are not well suited for use at the AHDR because they underestimated evaporation rate as shown in Fig. 3-9. In general, these approaches showed a low sensitivity for the input data.

3.3.2.4 Dalton group

Both methods based on Dalton theory and rely on the terms of U_2 and (e_0–e_a) in addition to (T_0–T_a) in case of Ryan–Harleman. The value of the mass transfer coefficient is specific for the characteristics of the site used to record the meteorological data (Finch and Calver 2008). Ryan-Harleman equation was developed to determine the evaporation from heated water bodies. In that case, both forced convection driven by wind and free convection driven by buoyancy control the evaporation rates, while for natural water bodies forced convection is the dominant factor (Dadaser-Celik and Stefan, 2008).The low values of the wind speed and the vapor pressure gradient explain the smaller rate of evaporation determined by both methods at Allaqi station. In general, mass transfer method is well suited for use because of its simplicity and reasonable accuracy.

3.3.2.5 Temperature group

The Papadak is method depends on the differences in the saturated vapor pressure above the water body at maximum and minimum air temperatures. Thornthwaite's method is based on the air temperature with an adjustment made for the number of daylight hours. So, it is logical that the evaporation rates increase when the air temperature increases. Fig. 3-9 shows that the seasonal amplitude between the minimum and maximum monthly evaporation rates determined by both approaches are different. This seasonal amplitude was estimated as 10 mm d^{-1} in case of Thornthwaite approach while it was 2 mm d^{-1} in case of the Papadakis method. Thornthwaite determined evaporation rates less than 2 mm d^{-1} in January and December at the three stations. These low rates are not well suited to the climate conditions of the AHDR. The higher values of air temperature at the Raft station explain the higher evaporation rate estimated at this station.

3.3.2.6 Temperature, day length group

Blaney-Criddle correlated monthly measured evaporation rate with monthly mean air temperature times the proportion of daylight hours to the total annual hours of the daylight to develop a monthly empirical evaporation coefficient (Majidi *et al.* 2015). Hamon formulated a simple equation to determine the potential evapotranspiration given mean air temperature and day length. It is often used to estimate lake evaporation because of its simplicity. As shown in Fig. 3-9, the evaporation rate determined at the three stations by Blaney-Criddle, as well as Hamon, are convergent because the daylight values at the three stations are comparable. The Hamon approach underestimated evaporation rates at the three stations.

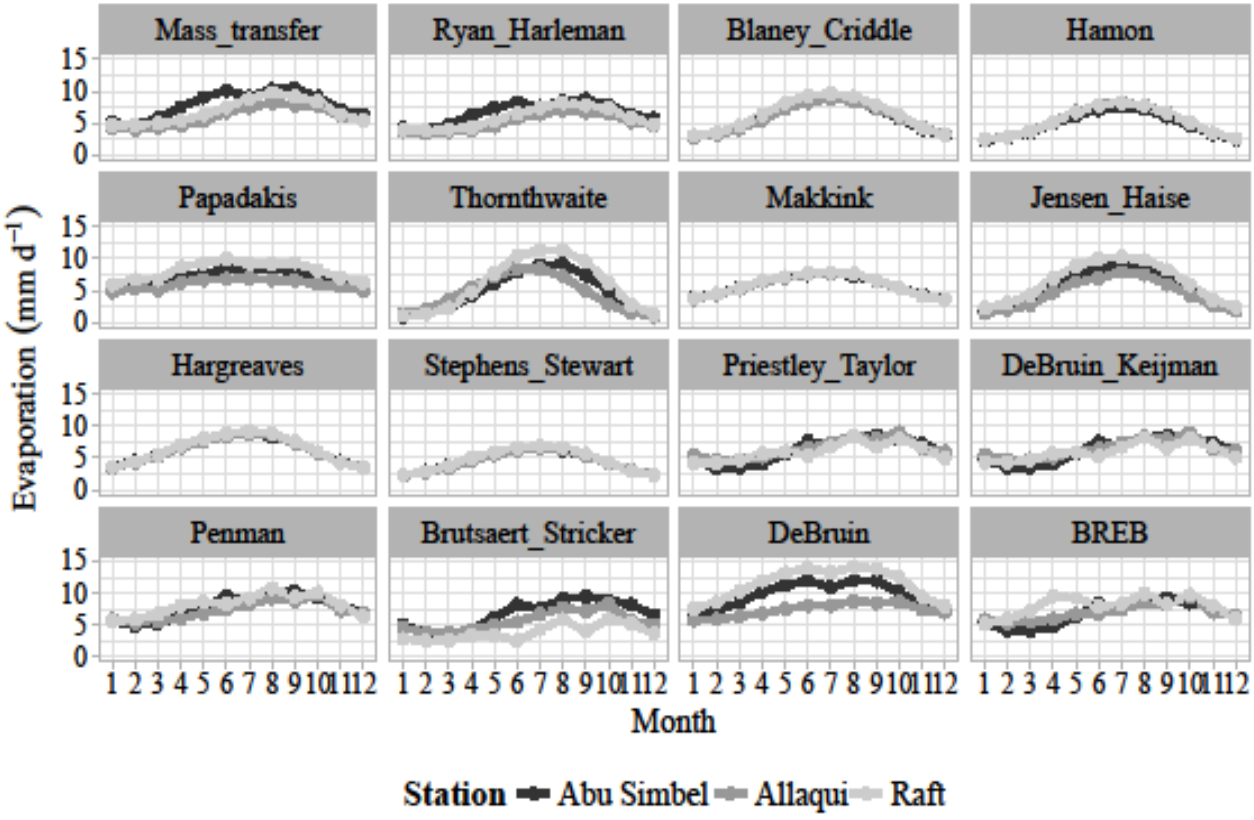

Figure 3-9 Daily evaporation values at the floating stations (mm d^{-1}) averaged per month as estimated by 16 evaporation methods listed in Table 1

Table 3-2. Mean monthly Bowen ratios (computed from daily values) at the three floating stations

Month	Floating stations		
	Abu-Simbel	Allaqi	Raft
January	0.059	0.050	-0.007
February	-0.035	0.076	-0.107
March	-0.079	0.002	-0.196
April	-0.075	-0.020	-0.318
May	-0.086	-0.045	-0.342
June	-0.077	-0.013	-0.283
July	-0.072	-0.002	-0.195
August	-0.079	-0.008	-0.146
September	-0.058	-0.006	-0.150
October	-0.017	0.001	-0.117
November	0.066	0.006	-0.062
December	0.112	0.023	-0.004

Table 3-3. Daily evaporation values at the floating stations (mm d^{-1}) averaged per year as estimated by 16 evaporation methods listed in Table 1

Method group	Method	Floating station		
		Abu-Simbel	Allaqi	Raft
Energy budget	BREB	6.7	6.9	7.9
Combination group	Priestley-Taylor	6.1	6.4	6.0
	DeBruin-Keijman	6.1	6.4	5.9
	Penman	7.7	7.3	8.1
	Brutsaert-Stricker	6.7	5.6	4.2
	DeBruin	9.7	7.4	11.4
Solar radiation, temperature group	Jensen-Haise	5.4	4.5	6.3
	Makkink	5.8	5.8	5.9
	Stephens-Stewart	4.4	4.4	4.6
	Hargreaves	6.3	6.2	6.4
Dalton group	Mass-transfer	7.2	6.0	6.8
	Ryan-Harleman	6.6	5.1	5.8
Temperature group	Papadakis	7.0	6.0	8.0
	Thornthwaite	4.8	4.5	5.8
Temperature, day length group	Blaney-Criddle	5.9	5.8	6.3
	Hamon	4.9	5.2	5.2

To measure the relation between the different methods, two measures are used: (1) the percentage root mean square error (%RMSE) and (2) the percentage mean absolute error (%MAE):

$$\%\mathrm{RMSE} = \sqrt{\frac{\sum(V_{modelled}-V_{obs})^2}{n}} \times \frac{100\times n}{\sum V_{obs}} \quad (8)$$

$$\%\mathrm{MAE} = \frac{\sum|V_{modelled}-V_{obs}|}{\sum V_{obs}} \times 100 \quad (9)$$

$V_{modelled}$ and V_{obs} are the evaporation rates determined by the approaches listed in Table 1 and evaporation rates determined by water balance method, respectively; n is the total number of observations.

As depicted in Fig. 3-10, the obtained values from %RMSE and %MAE are greater than 50%, which means a weak relation between the modelled and observed values. Also, Fig. 3-11 shows a systematic deviation between the monthly averages determined by water balance and the 16 approaches at the three floating stations. This deviation is clear in the months of May, June, July, and September.

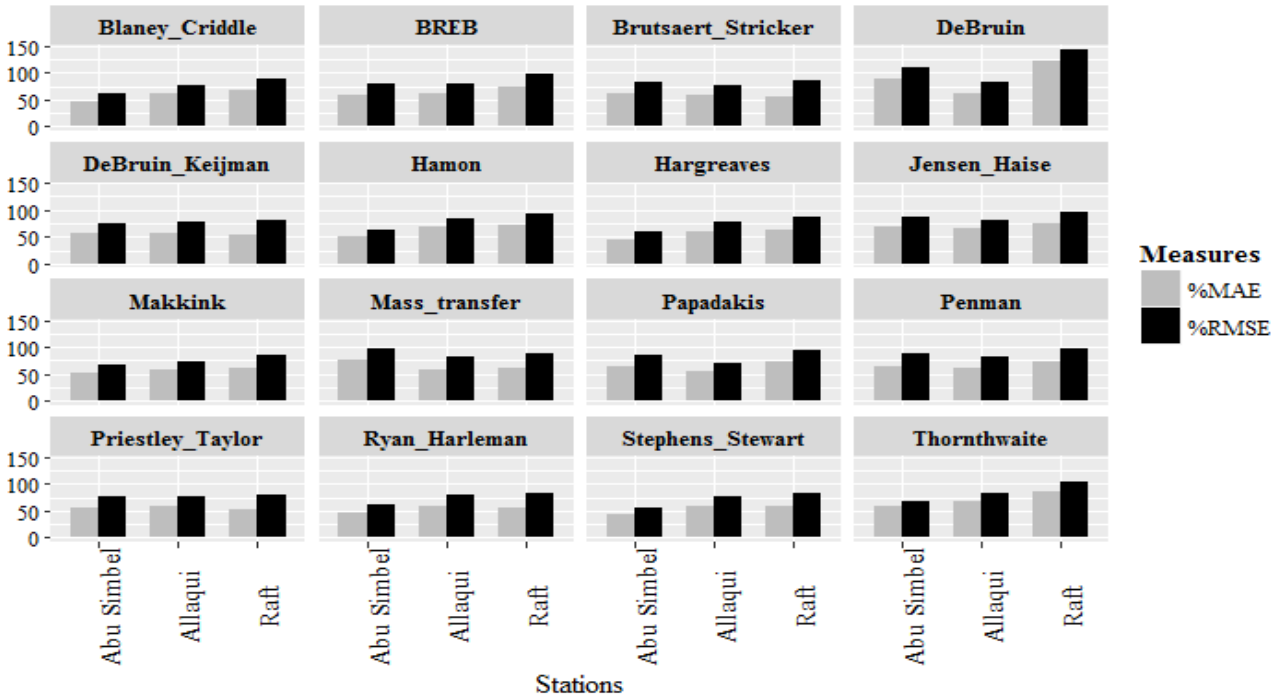

Figure 3-10 Evaporation rate comparison. Shown are the root-mean-square error (RMSE) and mean absolute error (MAE) as a percentage of the respective model estimate.

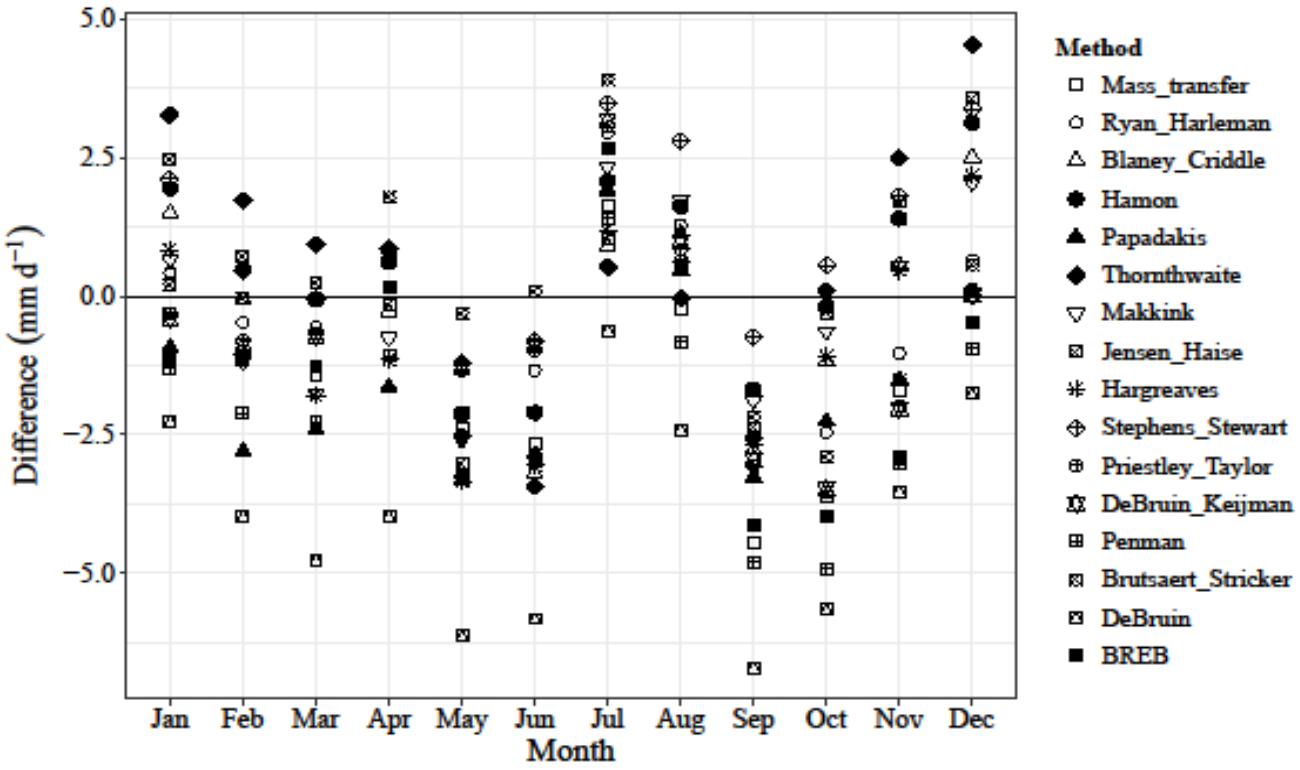

Figure 3-11 Monthly mean differences (mm d^{-1}) between evaporation calculated with 16 estimation methods and the water balance method as the reference for the period 1978 until 1984

3.4 Conclusions

The total annual water losses determined by the water balance method during the period from 1968/1969 to 2010/2011 amounted to 413 km^3, giving an average annual loss of 9.6 km^3 yr^{-1}. This means that the average annual water loss is around the designed value (10 km^3 yr^{-1}). The average annual evaporation rate determined by the water balance method during the period 1978–1984 is 5.5 mm d^{-1} with maximum evaporation in July (10.1 mm d^{-1}) and minimum evaporation in February (3.3 mm d^{-1}). Given the range of estimates derived from the different evaporation calculation methods, the average annual evaporation rate estimated by the water balance method, provides a realistic value of 5.5 mm d^{-1}. Some average monthly evaporation rates estimated by the water balance method, compared with alternative methods, are not appropriate. These inappropriate values are due to uncertainties and inaccuracies of the estimated inflow based on the upstream Dongola station. The BREB, which is considered the most accurate method, estimated the evaporation rate at the three floating stations Raft, Allagi and Abu Simbel at 7.9, 6.9 and 6.7 mm d^{-1}, respectively.

The highest evaporation rates at Raft station are due to the very negative values of the BR. Penman estimated relatively higher evaporation rates as compared to the BREB. Stephens-Stewart, Thornthwaite, Jensen-Haise, and Hamon approaches are not quite suitable for use at the AHDR because they severely underestimated evaporation rates obtained from the water balance reference method. De Bruin's approach overestimated evaporation rates at the Raft and Abu Simbel stations. All other approaches estimated realistic evaporation rates. The mass transfer method is considered the most appropriate method because of its simplicity, reasonable accuracy, and low sensitivity to input data. The solar radiation and temperature approaches also show a low sensitivity for input data.

The results of the study show systematic deviations between the monthly average values determined by water balance method over the period 1978–1984 and the monthly mean values determined by 16 approaches at the three floating stations. This deviation is clearest in the months of May, June, July, and September.

4-Seepage Loss from Nasser Lake

Journal article (to be submitted)
Authors: El-Shazli, A., Hörmann, G., Wagner, P.D., Fohrer, N.

4 Seepage Loss from Nasser Lake

Abstract:

Water losses by seepage to groundwater are a big problem in lakes like the Nasser Lake (NL). To monitor these losses, boreholes and control wells are installed around the lake. Unfortunately, these wells sometimes have no connection to the water level of the lakes due to the geological complexity of the underground. Cross-correlations (ccf) can be used to test the connection between the water level in the Nasser Lake (NL) and the groundwater table in the boreholes around the lake. The study found that there is a cross-correlation between the groundwater tables at some boreholes and the water levels in the NL of a reasonable significance value (a clear connection) for a time delay up to 100 days. Some boreholes have significant negative correlations, which means when the water levels in the NL decline the groundwater tables increase and vice versa. The holes with a connection with the water level of the lake were used to calculate the seepage from the lake with Darcy's law. We found a seepage of 47×10^6 m^3 yr^{-1} for the period 1996-2005 . This value represents less than 1% of the average annual flow of the Nile River into the AHDR for the period 1965–2010 which was estimated as 73×10^9 m^3.

Keywords: Nasser Lake; Boreholes; Groundwater table; Water levels; Cross-Correlation Function; Time delay.

4.1 Introduction

The interaction of ground water with adjacent surface water is an important aspect of hydrogeological systems (Barlow and Moench 1998). The groundwater is influenced by adjoining surface water systems, but sometimes it is difficult to monitor this influence. Lakes can have fluctuating levels, bank storage can be significant, and they have a continuous flushing of water through them (Winter et al. 1998).

Polemio and Casarano (2008) used cross-correlation (ccf) with a lag from 1-12 months to study the relation between piezometric data and temperature, rainfall and river discharge data for the period 1821 to 2003 in southern Italy. They found that there is a cross-correlation of up to 4 months between the piezometric and climatic parameters and 1-2 month between river discharge and piezometric level.

The designers of the Aswan High Dam Reservoir (AHDR) estimated the annual water loss from the lake at 10×10^9 m^3, of which 9×10^9 m^3 were evaporative losses. The average seepage loss was estimated at 1×10^9 m^3 yr^{-1} (Wafa and Labib 1973). Moreover, Wafa and Labib (1973) studied the seepage and absorption losses from the NL. For a porosity of the dry rock of 25% they calculated 48 km^3 of water to fill up the rock with a maximum seepage loss of 0.97×10^9 m^3 yr^{-1}.

Afifi and Osman (1993) used Darcy´s law to compute the annual seepage loss during the period from 1964/1965 to 1990/1991. They estimated the annual average value as 52×10^6 m^3 yr^{-1}

Metwaly et al. (2006) applied Darcy's law to estimate the seepage value from the lake to the adjacent Nubian sandstone aquifer. The study declared that the expected water seepage value is about 2.6×10^6 m^3 yr^{-1}.

Elsawwaf et al. (2014) used cross-sectional modeling based on the analytical solution of Edelman (1947) to study the groundwater–surface water interaction in NL. They used timeseries data of piezometric heads collected at the cross sections during the period 1965–2004. They estimated the total volume of recharge in the study area during the 40-year period at 48.1×10^9 m^3 (1.2×10^9 m^3 yr^{-1}).

Abdel-Moneim et al.,(2014) used piezometric data of six profiles of observation wells distributed along both sides of the lake to determine the seepage. The study indicated that the seepage loss was estimated, applying Darcy's law, as 0.24×10^9 m^3 yr^{-1}.

The objectives of this study are: (1) using cross-correlation between the groundwater tables in the boreholes and the water levels in the NL to find the boreholes with a connection to the water level in the NL; (2) to estimate the seepage volume from the NL to the groundwater using the 29 boreholes; (3) to estimate the volume of water, which is needed to saturate the dry rock.

4.2 Materials and methods

Nasser Lake (NL) is an artificial lake in southern Egypt. It represents the Egyptian part of the AHDR. The lake extends along 350 km between 22˚31' to 23˚45' N and 31˚30' to 33˚15' E (Entz 1976). It is situated in a typical arid area in the Nubian Desert (El Kobtan et al. 2016) above a layer of Nubian sandstone (Elsawwaf et al. 2012). The mean slope of the mountainous eastern shoreline of the lake is steeper than the flat and wide

western one (El Shahat 2000). The lake has an area of 5238 km² and an average width of 18 km at the elevation of 180 m a.s.l (Entz 1973).

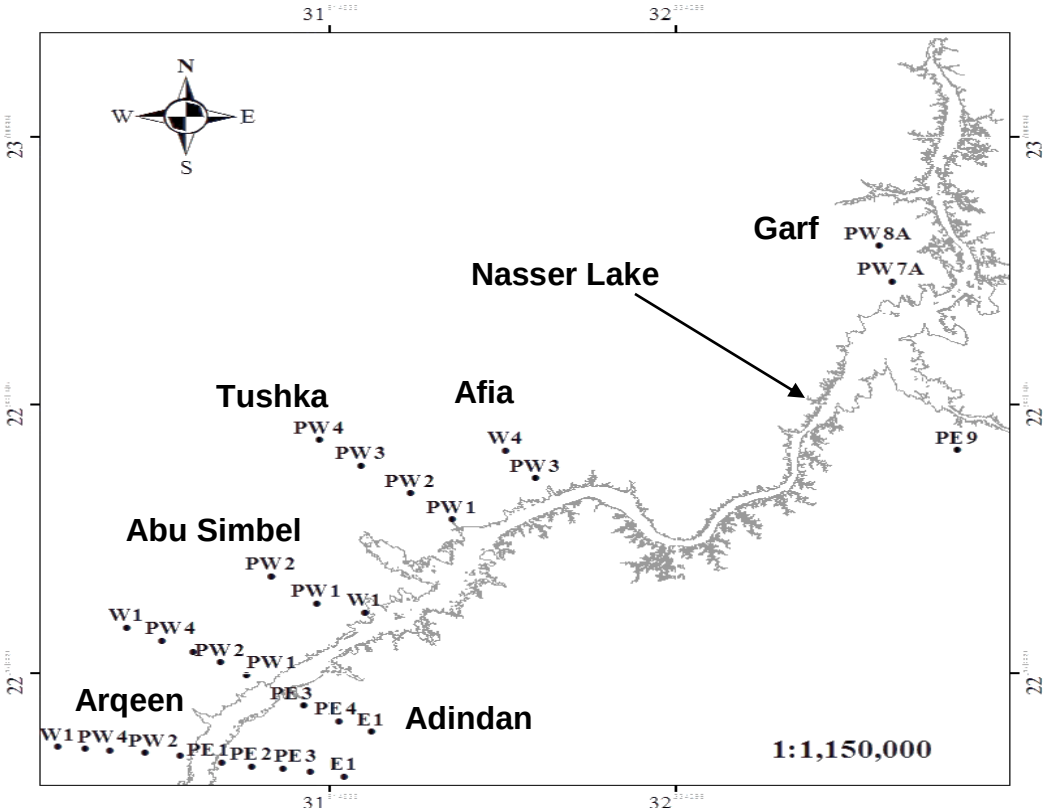

Figure. 4-1 Boreholes around the Nasser Lake

From a hydrogeological point of view, the Nubian sandstone formation is the main aquifer in the study area. It is the divided into four different layers with total thickness varying from 200 m to 580 m. The lowest unit consists of variegated clays overlying the granitic basement. The second layer is brownish shale and sandstone intercalated with clay. The third unit is a permeable sandstone water bearing formation and variegated shale. The uppermost unit is the phreatic aquifer, which is composed of sandstones with 25% – 30% porosity interspersed with claystone lenses. The river cuts into the sandstone strata. Therefore the water level of the lake and the groundwater table are related as depicted in Fig 4-2.

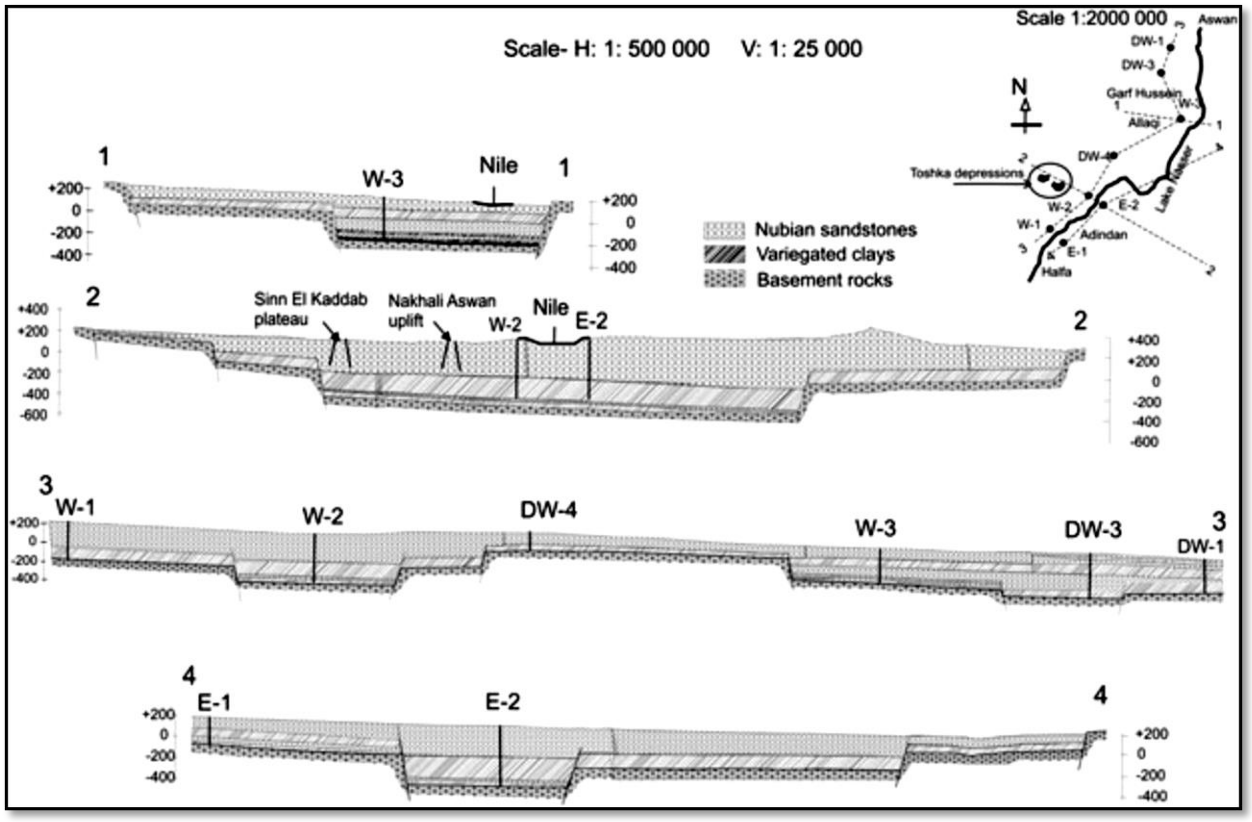

Figure. 4-2 Schematic geological cross-sections along the Nasser Lake (Elsawwaf et al. 2014)

To determine the interaction between the surface water and groundwater in the NL area, 25 shallow and 4 deep observation wells were installed. They are distributed along both sides of the lake at six cross-sections as shown in Fig. 4-3. These sectors are Garf Hussein, Afia, Tushka, Abu Simbel, Adindan, and Arqeen.

For this study, we used daily time series from 1996-2005 of the water level of the NL and the groundwater table obtained from observation wells around the lake. As depicted in Fig. 4-4 the time series data of Adindan boreholes which represent the period 1996-2005 has gaps. Borehole W1 at Abu Simbel recorded outlier values. The time series data of Tushka boreholes represents a period of less than one year. Boreholes at Arqeen (East) sector have time series data for more than one year. Some boreholes at sectors like Abu Simbel, Afia Arqeen (west) and Garf have time series data for reasonable periods without gaps.

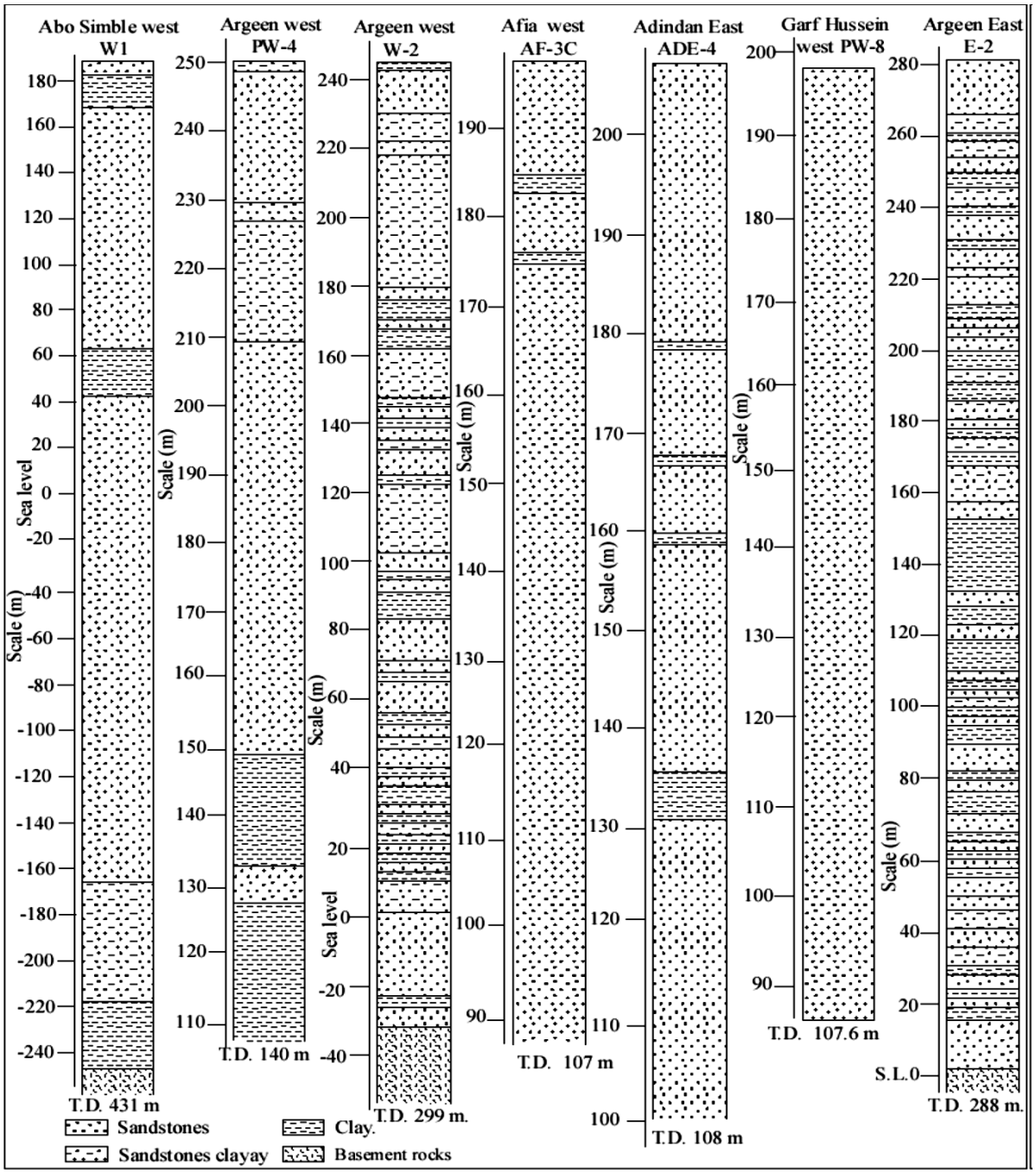

Figure. 4-3 Geological structure at some boreholes at sectors Abu Simbel,Adindan, Afia, Arqeen and Garf Hussein (Hamdan et.al 2013)

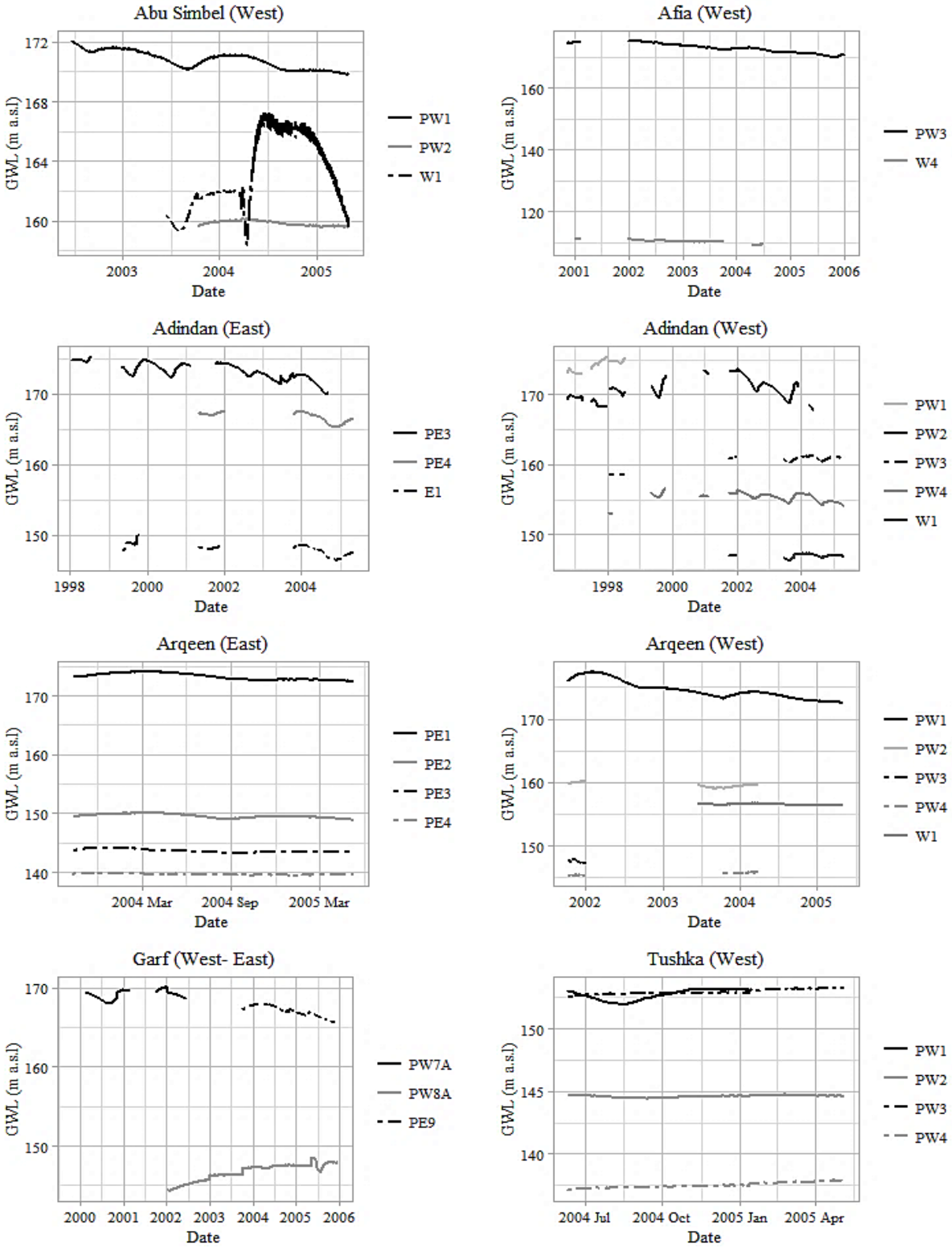

Figure. 4-4 the groundwater tables at the boreholes around the Nasser Lake

Table 4-1 The boreholes around the Nasser Lake

Sectors	Boreholes	Borehole depth (m)	Distance from the shoreline of the NL (m)	Sectors	Boreholes	Borehole depth (m)	Distance from the shoreline of the NL (m)
Garf	PW7A	102	2000	Afia	PW3	103.3	1500
	PW8A	107.6	3000		W4	211	6000
	PE9	97.4	1000	Abu Simbel	PW1	98.4	1000
Tushka	PW1	100	2000		PW2	95.0	3000
	PW2	98	4000		W1 (deep)	431	-
	PW3	111	6000	Adindan (West)	PW1	82.0	1000
	PW4	125	8000		PW2	97.0	3000
Adindan (East)	PE3	88.0	2000		PW3	114.6	5000
	PE4	107.9	3000		PW4	140.1	7000
	E1 (deep)	273.3	4000		W1 (deep)	390.3	8000
Arqeen (East)	PE1	66.1	1000	Arqeen (West)	PW1	100	1000
	PE2	105	3000		PW2	105	3000
	PE3	145	5000		PW3	120	5000
	PE4	165	7000		PW4	140	7000
					W1 (deep)	299	10000

Cross-correlation (ccf) with a maximum time lag of 200 days was used to detect the influence of water level fluctuation in the NL on the groundwater table in the boreholes. The cross-correlation at time delay *d* is determined using the following formula (Davis and Sampson 1986):

$$r_d = \frac{n\sum xy - \sum x \sum y}{\sqrt{(n\sum x^2 - \sum x)(n\sum y^2 - \sum y)}} \quad (1)$$

where, r_d is the cross correlation coefficient at time delay *d*; *d* is the time lag between two time series (days); *n* is the number of overlapping data points; *x* is the water level in the NL; *y* is the groundwater table in the boreholes. For the practical calculations, we used R, the software for statistic computing and data visualization.

Darcy's law is used to estimate the amount of lateral seepage flow from the NL to the groundwater. Darcy's law can be expressed as:

$$Q = K \cdot I \cdot A \quad (2)$$

$$I = \frac{\Delta h}{l} \quad (3)$$

$$A = H \times L \quad (4)$$

Where: Q is the discharge in $m^3\ d^{-1}$, I is the hydraulic gradient, K is the coefficient of permeability in m/day, A is the area of the flow in m^2, Δh is the difference between the

water levels in the lake and boreholes, and l is the distance between the lake shoreline and the successive boreholes, H is the thickness of the seepage face in m and L is the length of seepage face in m. The seepage per unit area depends on two factors, the coefficient of permeability of the formation and the hydraulic gradient. The first factor was obtained from field tests conducted by the MWRI. Results of the field tests are presented in Table 4-2. The second factor was calculated from the piezometeric readings.

Table 4-2. Hydraulic conductivity, thickness of the seepage face, and the seepage length.

Section	Permeability coefficient (m d^{-1})	Thickness of the seepage face (m)	Seepage length (km)
Garf (East)	0.355	95.70	100
Garf (West)	0.709	105.7	80
Afia	0.166	105.85	120
Tushka	0.154	204.00	30
Abu Simbel	0.086	204.00	42
Adindan (East)	0.173	204.00	180
Adindan (West)	0.086	204.00	28
Arqeen (East)	0.356	204.00	21
Arqeen (West)	0.356	204.00	21

Another fraction of water loss is the absorption of water by dry rock until the lake is filled to its maximum. These losses that result from the saturation of rock at different accumulation levels of the NL can be determined according to the following equation (Cedergren, 1998):

$$Q_{abs} = N * A \left[\frac{(W_1 + W_2)}{2} - 120\right] \quad (5)$$

Where Q_{abs} is the absorption (saturation) loss in km^3, A is the increase in the lake surface area because of the change of water level from W1 to W2 in km^2, W1 and W2 are the maximum water levels for two successive years in meter, and N is the average porosity of the soil estimated as 25% (Wafa and Labib, 1973).

4.3 Results and discussion

The cross-correlation values for a time lag of 200 days for all the boreholes around the NL are depicted in Fig 4-4. The cross correlations of water levels in the NL and groundwater level can reveal the relation between groundwater table response to the water level in the lake and delay time for a response.

As shown in Fig 4-5, the boreholes with a connection to the lake water level can be clearly identified. These boreholes are PW1 and PW2 at Abu Simbel sector, PW3 at Afia sector, PE3 and PE4 at Adindan (east) sector, PW2 at Adindan (west) sector, PE1 at Arqeen (east), PW1,PW2 and W1 at Arqeen (west), PW7 and PE1 at Garf (east-west) sector and PW1, PW2, PW3 and PW4 at Tushka (west) sector.

At Tushka sector, borehole PW1 has a direct connection to the lake water level. Boreholes PW2, PW3 and PW4 curves show the expected delayed response and PW3 and PW4 apparently match, although there is 2000 m distance between them.

The boreholes PE2, PE3, and PE4 at Arqeen east sector showed a positive correlation for a time delay less than PE1, although they are further away from the shoreline of the NL than PE1. The same issue was detected with boreholes PW2 and PW4 at the sector of Adindan (west), and there is no hydrological or geological reason to explain this case.

Some boreholes have negative correlations between groundwater tables in the boreholes and water levels. They represent periods when the two time-series data are out of phase (Lee, Lawrence, and Price 2006) and cannot be used for further analysis because there is no hydraulic connection between lake and ground water in the short run. The calculated seepage (Table. 4-3) varies between 0.039 $m^2\ d^{-1}$ at Adindan west to 0.743 $m^2\ d^{-1}$ at Garf west. The maximum seepage at Garf west is caused by the highest hydraulic conductivity and hydraulic gradient in this sector. The total seepage loss from 1996-2005 is estimated as $47\times10^6\ m^3\ yr^{-1}$.

Table 4-3. Average values of hydraulic gradient, discharge per unit area, and total discharge at different sectors.

Section	hydraulic gradient	q ($m^2\ d^{-1}$)	Q ($\times10^6\ m^3\ yr^{-1}$)
Garf (East)	0.007	0.25	9.13
Garf (West)	0.010	0.743	21.70
Afia	0.003	0.040	1.75
Tushka	0.007	0.231	2.53
Abu Simbel	0.004	0.120	1.84
Adindan (East)	0.005	0.087	5.72
Adindan (West)	0.002	0.039	0.40
Arqeen (East)	0.002	0.135	1.03
Arqeen (West)	0.005	0.380	2.91

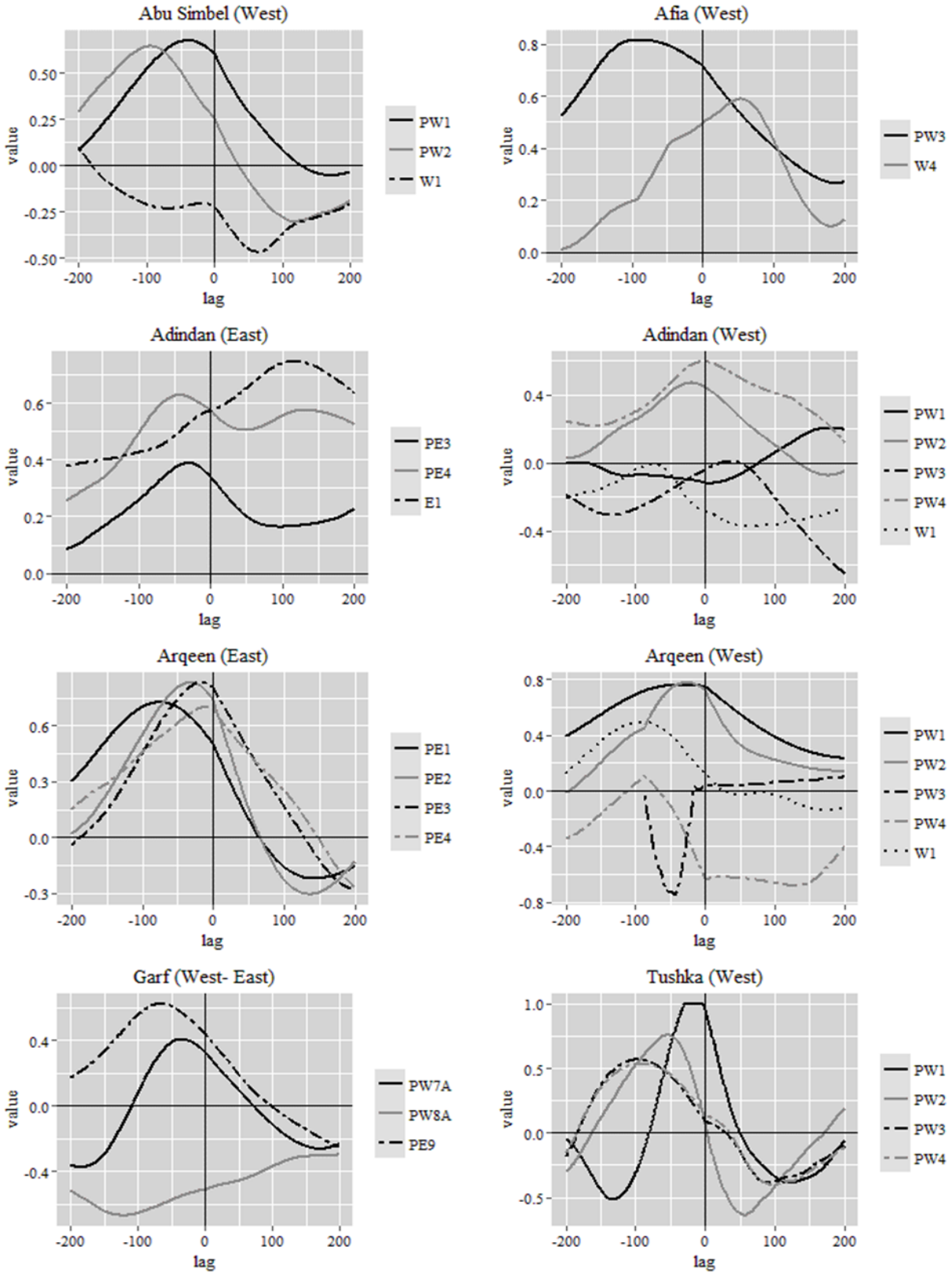

Figure. 4-5 Cross-correlation between daily water level in the Nasser Lake and groundwater table at the boreholes around the lake

The water level of the reservoir started to increase after the construction of the AHD in 1964. In 1975, the reservoir level reached the full storage level (175 m a.s.l.) and approached the maximum storage level in November 1999 (181.60 m a.s.l.). From 2002 up to 2012, the level fluctuated between 168 and 178 m a.s.l. (Fig. 4-6).

Table 4-3 shows the absorption losses until the maximum lake water level of 181.60 on 10th of November 1999. According to Table 4-3, the total absorption loss was estimated as 60×10^9 m^3 from 1964-1999. Wafa and Labib (1973) found a lower value of 48×10^9 m^3 without mentioning the formula which is used to estimate this value.

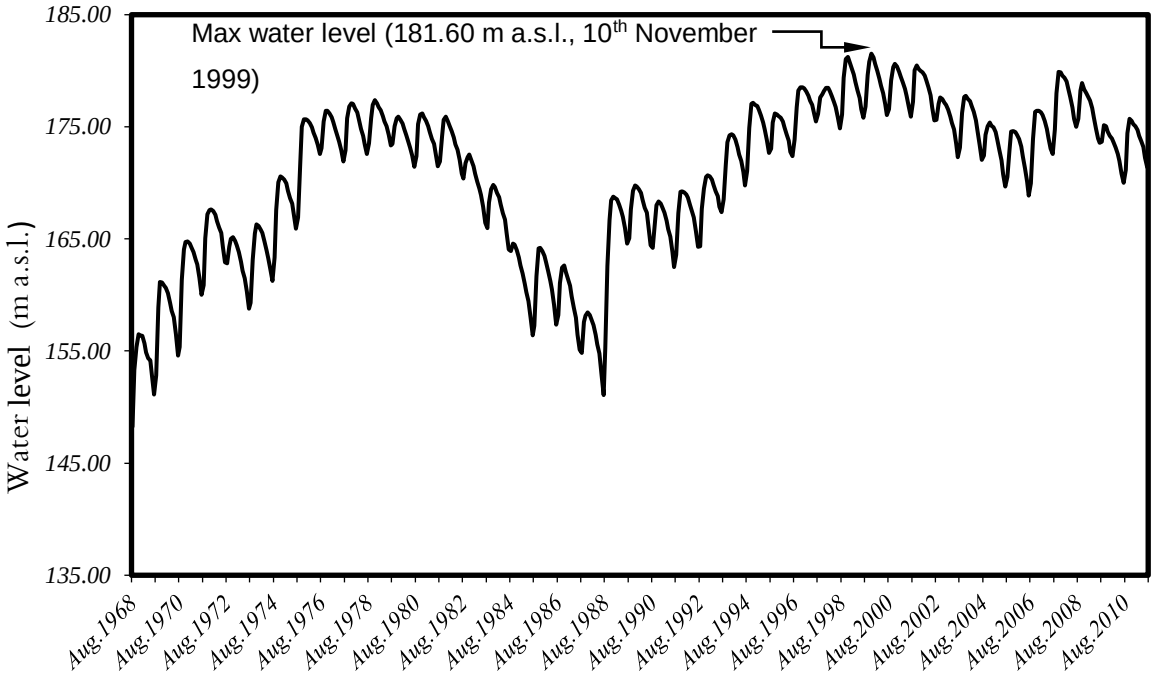

Figure. 4-6 Water level upstream AHD from 1968 till 2011 based on annual data from the MWRI

Table 4-4 Absorption losses at different water levels.

Water year	Max. Water level	Surface area (km^2)	NL Volume (km^3)	Saturated area (km^2)	Absorption loss (km^3)	$\left(\frac{\text{Absorption loss}}{\text{NL Volume}}\right)\%$
19964/65	127.60	690	9.62			
65/66	132.71	880	13.46	190	0.48	3.57
66/67	142.48	1415	24.50	535	2.35	9.59
67/68	151.22	2070	39.66	655	4.4	11.09
68/69	156.52	2580	51.85	510	4.32	8.33
69/70	161.23	3105	65.21	525	5.1	7.82

Water year	Max. Water level	Surface area (km^2)	NL Volume (km^3)	Saturated area (km^2)	Absorption loss (km^3)	$\left(\frac{\text{Absorption loss}}{\text{NL Volume}}\right)\%$
70/71	164.88	3565	77.47	460	4.95	6.39
71/72	167.64	3965	87.80	400	4.63	5.27
74/75	170.53	4400	99.88	435	5.34	5.35
75/76	175.71	5300	124.99	900	11.95	9.56
76/77	176.51	5450	129.25	150	2.10	1.62
77/78	177.21	5570	133.08	120	1.71	1.28
78/79	177.47	5630	134.53	60	0.86	0.64
96/97	178.54	5825	140.69	195	2.83	2.01
98/99	181.30	6420	157.75	595	8.91	5.65
99/2000	181.60	6456	159.70	36	0.55	0.34

4.4 Conclusions

The cross-correlation between the water levels in the NL and the groundwater tables at the boreholes shows that some boreholes have a connection with the NL and the other boreholes do not have a connection in the short run. There is a cross-correlation between the water levels in the NL and the groundwater tables at some boreholes of a reasonable significance value for a time delay up to 100 days. Some boreholes have significant negative correlations. These negative correlations represent an inverse relation between the water levels in the NL and the groundwater tables at some boreholes. The seepage values per unit area from the NL to the groundwater at the different cross sections ranged from 0.039 $m^2\ d^{-1}$, at Adindan west, to 0.743 $m^2\ d^{-1}$ at Garf west. The study showed that the average seepage value for the period 1996-2005 is about $47 \times 10^6\ m^3\ yr^{-1}$ which represents less than 1% of the average annual flow of the Nile River into the AHDR. This small value of the seepage is due to the very low values of the permeability coefficient of the banks rocks. The volume of water which is lost to saturate the dry rock in 35 years until the lake fills to the level of 181.60 m a.s.l is about $60 \times 10^9\ m^3$ with an average of $1.7 \times 10^9\ m^3\ yr^{-1}$, about 2.5% of the average annual flow of the Nile River into the AHDR . This value is comparetively high when compared to the seepage value.

5 Summary and Conclusions

The AHDR is a large human-made reservoir, and it was formed as a result of the construction of the AHD across the Nile River. It lies in southern Egypt and northern Sudan. The AHDR was designed to have a maximum water level of 182 m a.s.l., with a total storage capacity of 162 km^3. The length of the AHDR is about 500 km, 350 km in Egypt and the rest in Sudan, with an average width of 12 km.

The main components of the water balance for lakes and reservoirs are inflow, outflow and water loss by evaporation and infiltration. Water storage capacity (elevation- storage curve) is required to estimate the change of the water volume.

The water balance provides an indirect evaluation of unknown water balance components from the difference between the known items. In our case, the known items are inflow and outflow, and the unknown component is the water loss from the reservoir.

Studying the water balance of the AHDR requires examining three main points. These points are: (1) the change in the storage capacity of the AHDR because of sediment entry; (2) the evaporation rate from the reservoir; and (3) and the exchanged water volume between groundwater and surface water in the reservoir area.

Therefore, this study focused on three topics. The first is the change in the storage capacity of the AHDR, due to sedimentation, and the generation of a new elevation–storage capacity curve that represents the present storage capacity. The second topic is estimating the evaporation rate from the AHDR. The third topic is about the seepage and absorption loss.

The first chapter examines the change in the storage capacity and the morphology of the AHDR using Landsat imagery, bathymetric data and digital contour map of the AHDR area before the dam construction.

The results indicate that the total storage capacity of the AHDR decreased by 12%. This decrease was mainly in the live and dead storage capacity zone, and slightly in the flood control zone. The change in storage capacity led to a new elevation-capacity curve. The new storage curve guarantees the water demands for irrigation, hydropower and water supply. The live storage capacity still meets the annual downstream requirements for water (Egypt's annual agreed quota from the Nile River is 55.5 km^3)

The second chapter discusses the evaporation rate from the AHDR, determined by the water balance method and alternative evaporation/evapotranspiration estimation methods. The meteorological data was obtained from three floating stations distributed along the reservoir. The study findings indicate that the total annual water losses determined by the water balance method during the period from 1968/1969 to 2010/2011 amounted to 413 km^3, giving an average annual value of 9.6 km^3. The average annual evaporation rate determined by the water balance method during the period 1978 - 1984 was 5.5 mm d^{-1}. Some of the alternative approaches determined a higher evaporation rate than the water balance method. Moreover, some of the alternative approaches like Stephens-Stewart, Thornthwaite, Jensen-Haise, and Hamon are not quite suitable for use at the AHDR because they severely underestimated or evaporation rates.

In the third chapter the seepage loss and absorption loss from the AHDR was discussed. Daily time series from 1996-2005 of the water level of the AHDR and the groundwater table obtained from 29 observation wells that were installed around the reservoir were analysed.

The results show that the average seepage value for the period 1996-2005 is about 47×10^6 m^3 yr^{-1} which represents less than 1% of the average annual flow of the Nile River into the AHDR. Also, the results indicate that the volume of water which is lost to saturate the dry rock in 35 years is about 60×10^9 m^3 with an average of 1.7×10^9 m^3 yr^{-1}, which is about 2.5% of the average annual flow of the Nile River into the AHDR.

The main conclusions of this study can be summarised as follows:

- The water balance method, which was used to estimate the water loss, was not affected by the changes in the storage capacity of the reservoir. This is due to the fact that the fluctuation of the water level lies in a zone that is only slightly exposed to sedimentation (the flood control and the upper part of the live storage zone).
- The water balance method is strongly affected by the inaccurately estimated inflows based on the upstream station Dongola.

- The AHDR is very large, and every part of it has a different meteorological conditions resulting in evaporation rates.
- The water loss by evaporation at the water level of 175 m a.s.l., was estimated by some alternative approaches, like Penman, mass transfer, Priestly Taylor and BREB in a range of 12 to 16 $km^3\,yr^{-1}$, which is higher than the designed value (10 $km^3\,yr^{-1}$).
- The average seepage value for the period 1996-2005 is very low when compared to the evaporation loss.
- There is no absorption loss after the lake fills to the level of 181.60 m a.s.l in the hydrological year 1999/2000. This is due to the fact that the water levels were lower than the level of 181.60 m a.s.l., which also means that the main water loss is due to evaporation.

6 Recommendations

This study is an attempt to get an accurate view of the hydrological aspects of the reservoir area, and an accurate estimate of the different terms of the hydrological budget. Based on its results, the following measures can be recommended:

- The meteorological stations and their distribution along the lake are not sufficient to determine a precise evaporation rate for the entire reservoir. So, additional meteorological stations on the reservoir need to be established to collect more meteorological data, which in turn, could then be used in follow-up studies.
- The meteorological stations should be maintained periodically to avoid losing a lot of meteorological data.
- Establishing an automatic hydrometeorological network covering the reservoir would be necessary to get a more accurate assessment of the evaporation rate
- Remote sensing data, in particular satellite imagery with high resolution like GeoEye-1 50cm Global High-Resolution Satellite Imagery, should be used to detect the changes in the reservoir because of sediments. In addition to meteorological ground data, satellite data can be used to estimate the evaporation rate.
- Additional boreholes should be installed around the reservoir to get a clear view of the interaction between groundwater and surface water.
- A flow and sediment load gauging station close to the reservoir entrance should be established to get an accurate and continuous inflow and sediment load measurements.
- Another new location should be used to measure the discharges of the Main Nile to alleviate the sedimentation problems at Dongola station.
- Detailed feasibility studies of alternative operating systems of the reservoir should be conducted to reduce the evaporation loss. For Example, the water elevation at the starting of flood season, August 1st, could be 170 m a.s.l. instead of 175 m a.s.l. to reduce the surface area of the AHDR. This leads to a reduction of evaporation loss.
- A feasibility study of the optimal methods to reduce sediment deposits from the AHDR needs to be conducted as well. A suitable method for the case of the

AHDR would be the manual dredging method. By this means, the sediment can be excavated by suction dredgers, hydraulic excavators after lowering the reservoirs water level. The excavated sediment can be used to cultivate the desert which surrounds the reservoir.

- As the floods bring a huge amount of sediment every year, the entire reservoir in particular the northern portion needs to be surveyed as accurately as the southern portion in order to update the DEM.

7 References

Abbasi, A., & Giesen, N. (2012, April). Evaporation Modeling in Lakes in Arid and Semi-arid Regions. In EGU General Assembly Conference Abstracts (Vol. 14).

Abileah, R., Vignudelli, S., & Scozzari, A. (2011). A completely remote sensing approach to monitoring reservoirs water volume. Int. Water Technol. J, 1, 63-77.

Abu El-Ata, A. (1978). Egypt and the Nile after the High Aswan Dam. Ministry of Irrigation and Land Reclamation, Egypt.

Abu-Zeid, M. A., & El-Shibini, F. Z. (1997). Egypt's high Aswan dam. International Journal of Water Resources Development, 13(2), 209-218.

Afifi, A. and H. Osman. 1993: International Symposium on High Aswan Dam Vital Achievements, Fully Controlled.

Allen, R. G., Pereira, L. S., Raes, D., & Smith, M. (1998). Crop evapotranspiration-Guidelines for computing crop water requirements-FAO Irrigation and drainage paper 56. FAO, Rome, 300(9), D05109.

ArcGIS, E. S. R. I. (2014). 10.2. 1 for Desktop. Redlands, CA: Environmental System Research Institute.

Barlow, P. M., & Moench, A. F. (1998). Analytical solutions and computer programs for hydraulic interaction of stream-aquifer systems (No. 98-415-A). US Dept. of the Interior, US Geological Survey; Information Services [distributor],

Cedergren, H. R. (1989). *Seepage, drainage, and flow nets*. Wiley.

Brutsaert, W. (2013). Evaporation into the atmosphere: theory, history and applications (Vol. 1). Springer Science & Business Media.

Brutsaert, W., & Stricker, H. (1979). An advection-aridity approach to estimate actual regional evapotranspiration. Water resources research, 15(2), 443-450.

Davis, J. C. (1986). Statistical and data analysis in geology. J. Wiley.

De Bruin, H. A. R. (1982). Temperature and energy balance of a water reservoir determined from standard weather data of a land station. Journal of Hydrology, 59(3-4), 261-274.

De Bruin, H. A. R., & Keijman, J. Q. (1979). The Priestley-Taylor evaporation model applied to a large, shallow lake in the Netherlands. Journal of Applied Meteorology, 18(7), 898-903.

Delclaux, F., Coudrain, A., & Condom, T. (2007). Evaporation estimation on Lake Titicaca: a synthesis review and modelling. Hydrological Processes, 21(13), 1664-1677.

El Shahat, M. 2000: Lake Nasser Overview. (J.F. Craig, Ed.) Sustainable fish production in Lake Nasser: ecological basis and management policy. The International Centre for Living Aquatic Resources Management.

Elba, E., Farghaly, D., & Urban, B. (2014). Modeling high Aswan Dam reservoir morphology using remote sensing to reduce evaporation. International Journal of Geosciences, 5(02), 156.

ElKobtan, H., Salem, M., Attia, K., Ahmed, S., Abou El-Magd, I., Tang, X., El-Magd, I. A. (2016). Sedimentological study of Lake Nasser; Egypt, using integrated improved techniques of core sampling, X-ray diffraction and GIS platform. *Cogent Geoscience*, *2*(1), 1168069. http://doi.org/10.1080/23312041.2016.1168069

El-Manadely, M. S., Abdel-Bary, R. M., El-Sammany, M. S., & Ahmed, T. A. (2002). Characteristics of the delta formation resulting from sediment deposition in Lake Nasser, Egypt: Approach to tracing lake delta formation. Lakes & Reservoirs: Research & Management, 7(2), 81-86.

Elsawwaf, M., Feyen, J., Batelaan, O., & Bakr, M. (2014). Groundwater–surface water interaction in lake Nasser, Southern Egypt. Hydrological Processes, 28(3), 414-430.

Elsawwaf, M., Willems, P., Pagano, A., & Berlamont, J. (2010). Evaporation estimates from Nasser Lake, Egypt, based on three floating station data and Bowen ratio energy budget. Theoretical and applied climatology, 100(3-4), 439-465.

Elsawwaf, M., Willems, P., & Feyen, J. (2010). Assessment of the sensitivity and prediction uncertainty of evaporation models applied to Nasser Lake, Egypt. Journal of Hydrology, 395(1-2), 10-22.

Elshemy, M. M. (2011). Water Quality Modeling of Large Reservoirs in Semi-arid Regions under Climate Change: Example Lake Nasser (Egypt) (Doctoral dissertation).

Entz, B. (1976). Lake Nasser and Lake Nubia. In The Nile, Biology of an Ancient River (pp. 271-298). Springer, Dordrecht.

Hamdan, A. M., Selim, S. A., & Zaki, M. (2015). Estimation of Seepage Loss from Nasser Lake to the Adjacent Nubian Sandstone Aquifer , Southern, *4*(9), 1106–

1116.

Finch, J., & Calver, A. (2008). Methods for the quantification of evaporation from lakes. Report, (October), 47.

Gao, H., Birkett, C., & Lettenmaier, D. P. (2012). Global monitoring of large reservoir storage from satellite remote sensing. Water Resources Research, 48(9).

Goel, M. K., Jain, S. K., & Agarwal, P. K. (2002). Assessment of sediment deposition rate in Bargi Reservoir using digital image processing. Hydrological sciences journal, 47(S1), S81-S92.

Goldsmith, E., & Hilyard, N. (1986). The Social and Environmental Effects of Large Dams: Volume 2; Case Studies. Wadebridge Ecological Centre.

Harbeck, G. E. (1958). Water-loss investigations: Lake Mead studies (Vol. 298). US Government Printing Office.

Henderson-Sellers, B. (1986). Calculating the surface energy balance for lake and reservoir modeling: A review. Reviews of Geophysics, 24(3), 625-649.

Ibrahim, S. A., El-Belasy, A., & Abdel-Haleem, F. S. (2011). Prediction of breach formation through the Aswan High Dam and subsequent flooding downstream. Nile Water Science and Engineering Journal, 4(1), 99-111.

Jain, S. K., Singh, P., & Seth, S. M. (2002). Assessment of sedimentation in Bhakra Reservoir in the western Himalayan region using remotely sensed data. Hydrological Sciences Journal, 47(2), 203-212.

Jorgensen, S. E., Loffler, H., Rast, W., & Straskraba, M. (2005). Lake and reservoir management (Vol. 54). Elsevier.

Lee, L. J. E., Lawrence, D. S. L., & Price, M. (2006). Analysis of water-level response to rainfall and implications for recharge pathways in the Chalk aquifer, SE England. Journal of hydrology, 330(3-4), 604-620.

Majidi, M., Alizadeh, A., Farid, A., & Vazifedoust, M. (2015). Estimating evaporation from lakes and reservoirs under limited data condition in a semi-arid region. Water resources management, 29(10), 3711-3733.

Metwaly, M., Khalil, M., Al-Sayed, E. S., & Osman, S. (2006). A hydrogeophysical study to estimate water seepage from northwestern Lake Nasser, Egypt. Journal of Geophysics and Engineering, 3(1), 21.

Mobasher, A. M. A. (2010). Adaptive reservoir operation strategies under changing boundary conditions–the case of Aswan High Dam Reservoir(Doctoral dissertation, Technische Universität).

Moneim, A. A. A., Zaki, S., & Diab, M. (2014). Groundwater Conditions and the Geoenvironmental Impacts of the Recent Development in the South Eastern Part of the Western Desert of Egypt. Journal of Water Resource and Protection, 6(04), 381.

Nilsson, C., Reidy, C. A., Dynesius, M., & Revenga, C. (2005). Fragmentation and flow regulation of the world's large river systems. Science, 308(5720), 405-408.

Ohmura, A. (1982). Objective criteria for rejecting data for Bowen ratio flux calculations. Journal of Applied Meteorology, 21(4), 595-598.

Omar, M. H., & El-Bakry, M. M. (1981). Estimation of evaporation from the lake of the Aswan High Dam (Lake Nasser) based on measurements over the lake. Agricultural Meteorology, 23, 293-308.

Palmieri, A., Shah, F., & Dinar, A. (2001). Economics of reservoir sedimentation and sustainable management of dams. Journal of environmental management, 61(2), 149-163.

Polemio, M., & Casarano, D. (2008). Climate change, drought and groundwater availability in southern Italy. *Geological Society, London, Special Publications*, *288*(1), 39–51.

Priestley, C. H. B., & Taylor, R. J. (1972). On the assessment of surface heat flux and evaporation using large-scale parameters. Monthly weather review, 100(2), 81-92.

Rango, A. (1994). Application of remote sensing methods to hydrology and water resources. Hydrological Sciences Journal, 39(4), 309-320.

Rao, L. Y., Sun, G., Ford, C. R., & Vose, J. M. (2011). Modeling potential evapotranspiration of two forested watersheds in the southern Appalachians. Transactions of the ASABE, 54(6), 2067-2078.

Rasmussen, A. H., Hondzo, M., & Stefan, H. G. (1995). A test of several evaporation equations for water temperature simulations in lakes. JAWRA Journal of the American Water Resources Association, 31(6), 1023-1028.

Rosenberry, D. O., Winter, T. C., Buso, D. C., & Likens, G. E. (2007). Comparison of 15 evaporation methods applied to a small mountain lake in the northeastern USA. Journal of Hydrology, 340(3-4), 149-166.

Sadek, M. F., Shahin, M. M., & Stigter, C. J. (1997). Evaporation from the reservoir of the High Aswan Dam, Egypt: A new comparison of relevant methods with limited data. Theoretical and Applied Climatology, 56(1-2), 57-66.

Said, R. (2013). The River Nile: geology, hydrology and utilization. Elsevier.

Schleiss, A. J., De Cesare, G., Franca, M. J., & Pfister, M. (Eds.). (2014). Reservoir sedimentation. CRC Press.

Shahin, M. M. (1985). Hydrology of the Nile basin (Vol. 21). Elsevier.

Shiklomanov, I. A. (1998). World water resources. A new appraisal and assessment for the 21st century.

Smith, S. E., Mancy, K.H., Latif, K. H., & Fosnight, E. A. (1983). Assessment and monitoring of sedimentation in the Aswan High Dam Reservoir using Landsat imagery. Hydrological Applications of Remote Sensing and Remote Data Transmission (Proceedings of the Hamburg Symposium, August 1983). IAHS Publ. no. 145, 499–508.

Sokolov, A. A., & Chapman, T. G. (1974). Methods for water balance computations; an international guide for research and practice-A contribution to the International Hydrological Decade.

Takeuchi, K. (Ed.). (1998). Sustainable reservoir development and management (No. 251). International Association of Hydrological Sciences.

Votruba, L., & Broža, V. (1989). Water management in reservoirs (Vol. 33). Elsevier.

Wafa, T. A., & Labib, A. H. (1973). Seepage losses from lake Nasser. Man-made lakes: their problems and environmental effects, 287-291.

Ward, A. D., & Trimble, S. W. (2003). Environmental hydrology. CRC Press.

Watson, I. (1993). Hydrology: An environmental approach. CRC Press.

World Commission on Dams. (2000). Dams and Development: A New Framework for Decision-making: the Report of the World Commission on Dams. Earthscan.

Whittington, D., & Guariso, G. (1983). Water management models in practice: a case study of the Aswan High Dam. Elsevier Scientific Publishing Company.

Winter, T. C. (1981). Uncertainties in estimating the water balance of lakes. JAWRA Journal of the American Water Resources Association, 17(1), 82-115.

Winter, T. C. (1998). Ground water and surface water: a single resource (Vol. 1139). DIANE Publishing Inc.

Wisser, D., Frolking, S., Hagen, S., & Bierkens, M. F. (2013). Beyond peak reservoir storage? A global estimate of declining water storage capacity in large reservoirs. Water Resources Research, 49(9), 5732-5739.

Woodward, J. C., Macklin, M. G., Krom, M. D., Williams, M. A., & Gupta, A. (2007). The Nile: evolution, Quaternary river environments and material fluxes. Large rivers: geomorphology and management, 13, 712.

WRRI, 2007. Using Remote Sensing and Numerical Modeling Techniques to Evaluate Lake Nasser Storage Capacity for Better Management. The Ministry of Water Resources and Irrigation, Cairo.

Xu, C. Y., & Singh, V. P. (2000). Evaluation and generalization of radiation-based methods for calculating evaporation. Hydrological processes, 14(2), 339-349.

8 Declaration

I declare and certify that apart from the supervisor's guidance the content and design of the thesis entitled Water balance of the Aswan High Dam Reservoir is entirely the result of my own work. I have faithfully and accurately cited all my sources, including books, journals, and unpublished manuscripts, as well as any other media, such as the Internet, letters or significant personal communication.

No part of this thesis has been submitted for a degree or a qualification at any other University or institution.

I confirm that my thesis has not been published – apart from the sub-publications mentioned below - and I will not make such a publication before the completion of the doctoral process.

The work was done under the guidance of Professor Nicola Fohrer, at the Institute of Natural Resource Conservation, Department of Hydrology and Water Resources Management. Kiel University.

The sub-publications are:

1- El-Shazli, A., & Hoermann, G. (2016). Development of storage capacity and morphology of the Aswan High Dam Reservoir. Hydrological Sciences Journal, 61(14), 2639-2648.

2- El-Shazli, A., Hoermann, G., Wagner, P.D., Fohrer, N. (2018). Comparison of water balance method and alternative evaporation methods applied to the High Aswan Dam Reservoir. Die Erde Journal, accepted.

Kiel, 6 .July, 2018 Ahmed El.Shazli

Ahmed